scientific reports

Check for updates

OPEN

Effect of biochar reinforcement on the mechanical and corrosion behavior of closed-cell aluminum foams

Ahmed Hassan & Ibrahim Abdullah Alnaser✉

Aluminum foam, a lightweight, energy-absorbing material with excellent thermal and mechanical properties, could be used in aerospace, automotive, and structural industries. To improve properties such as strength, wear resistance, and corrosion resistance, biochar, a sustainable resource derived from biomass pyrolysis, could be used as reinforcement. This paper reports the first use of Conocarpus biochar to reinforce closed-cell aluminum foams via the liquid metallurgy route. The aluminum foam samples were produced with different weight percentages of biochar (1 wt.%, 2 wt.%, 3 wt.%, and 4 wt.%), with fixed percentages of optimized composition from our previous study, 3% $CaCO_3$, 1%Al_2O_3 (AF02). This study examined mechanical and electrochemical characterization, morphology, density assessment, microhardness, and specific wear rate. In this paper, it was observed that the average pore size gradually increases when biochar is added to aluminum foam; it goes from 2.077 mm in AFB01 to 2.649 mm in AFB04 (4% biochar), a 27.5% increase. However, incorporating 4% biochar produces foam cell collapse, leading to elongated pores and collapsed struts. XRD studies show the proper distribution and intermetallic compound formation in biochar-reinforced aluminum foam. When biochar is added to aluminum foam, samples AFB01 to AFB03 have a lower relative density and higher porosity. The porosity escalates from 78.9% (AF02) to 86.74% (AFB03), whereas the relative density reduces from 21.1% (AF02) to 13.26% (AFB03). The compressive strength of foam significantly deteriorates when the concentration of biochar increases from 1 to 3%. In comparison to the base sample AF02, compressive offset stress decreases by up to 43.4% (AFB03), plateau stress decreases by 66.7% (AFB03), and energy absorption decreases by 68.8% (AFB03). The incorporation of biochar notably enhances the corrosion resistance of aluminum foam composites. Specifically, AFB01 (1% biochar) demonstrates an 88.8% improvement, while AFB03 (3% biochar) exhibits a 72.2% enhancement compared to the base sample, AF02. Conversely, the specific wear rate of AFB03 shows a deterioration of 39.7% relative to AF02. In terms of microhardness, AFB01 displays a slight increase of 5.88%, whereas AFB02 and AFB03 exhibit negligible variation when compared to AF02.

Keywords Aluminum foam, Sustainable, Biochar, Compressive properties, Corrosion resistant

Modern engineering applications need the development of new materials with higher mechanical qualities and corrosion resistance, especially in the structural, automotive, and aerospace industries, where efficiency and durability are critical. Since their introduction in the 1920s[1], metallic foams have become a transformational solution because of their distinct solid cellular structure with linked pores. These materials combine outstanding energy absorption[2], acoustic damping[3] high compressive strength, low density, and superior thermal conductivity[4]. Their superiority over conventional materials is due to their increased stiffness and hardness[5], and structural stability. Automotive engineering uses metallic foams for crash safety and lightweight designs, aerospace for weight reduction and impact resistance, and biomedical for bioimplants that mirror the porosity of real bone. Their use in infrastructure, military technologies, and heat exchangers underscores their importance as a future-oriented material for complex engineering problems. Materials science has focused increasingly on the development of unique materials to break down and liberate the limitations of conventional materials and develop an entirely novel perspective. Increasingly, engineers and scientists are also focusing on developing sustainable materials to improve the functionality, performance, and durability of a product. The mission of

Department of Mechanical Engineering, College of Engineering Riyadh, King Saud University, 11451 Riyadh, Riyadh Province, Saudi Arabia. ✉email: ianaser@ksu.edu.sa

such types of materials deals with a lesser impact on the environment and qualifies for better characteristics such as higher strength, less weight, better thermal stability, and enhanced corrosion resistance. Such revolutionary materials, with combined renewability and environment-friendly technologies, are meant to serve in aerospace, automotive, and energy industries, among others. Such research into sustainable materials should facilitate a more resilient, ecologically responsible future in addition to driving technical advancement[6]. The incorporation of sustainable reinforcements is a major precedence in contemporary studies, matching the worldwide demand for sustainable engineering solutions. In a variety of sectors, bio-products made from biomass resources provide sustainable substitutes. Among them, biochar has drawn a lot of interest due to its possible uses in waste management, carbon sequestration, and agriculture[7]. Biochar is now being studied for its potential to improve the mechanical characteristics of engineering materials, in addition to its traditional use in soil amendment and carbon capture. Biochar is regarded as the perfect reinforcing material for conventional materials because of its special qualities, which include high surface area, porosity, and chemical stability. This paper offers a thorough examination of aluminum foam reinforced with biochar, an environmentally beneficial and renewable addition, examining how it could improve material qualities and encourage sustainability throughout manufacturing engineering and other industrial applications[8–12].

Metallic foam can be produced using techniques such as liquid metallurgy, powder metallurgy, metal vapor deposition, and metal ion solution processing. They can be made with open or closed cells, with open-cell types typically produced using powder metallurgy, while closed-cell aluminum foam can be manufactured using the liquid metallurgy route. Aluminum foam, known for its non-toxic, light, and recyclable properties, has gained popularity in various industrial applications due to its low density and good construction. Closed-cell foams are used for impact and energy absorption, vibration control, and mechanical damping, while open-cell foams are lightweight and used in heat exchangers, filters, and implants.[13–15]. Closed-cell aluminum foam is produced in liquid metallurgy through blowing agents or melt gas injection. The process involves melting aluminum, adding a thickening agent, and creating bubbles. The properties of the foam are influenced by the amount of thickening and foaming agents, stirring speed, foaming time, and pre-foaming temperature[15–17]. Researchers have proposed different thickening agents, including Ca, SiC, Al_2O_3, Si_3N_4, TiB_2, and fly ash, to improve the viscosity of melts[15]. TiH_2, a common blowing agent for aluminum foam production, releases titanium and hydrogen gas upon decomposition, but is expensive, requires coating, is hazardous, flammable, and generates excess gas[18–21]. Researchers recommend employing carbonates instead of standard agents for aluminum foam synthesis since they emit CO_2 gas during decomposition, making foam manufacture more cost-effective, accessible, and manageable[16,22,23].

Biban et al.[24] studied the wear characteristics of bagasse biochar-reinforced epoxy composites. Biochar was mixed in different quantities with epoxy resin to investigate adhesion qualities and interfacial strength. Wear and adhesion tests were carried out to improve performance. Taguchi and DOE study discovered optimal process parameters. Abdo et al.[7] incorporate biochar into LDPE, and the findings demonstrate that biochar increases tensile strength by 1.9%, flexural strength by 47%, and hardness by 24.3%. It also reduces the melt flow index and friction coefficient by 56.3%, making biochar a feasible, environmentally acceptable additive for LDPE-based bio-composites. Zhang et al.[25] created a novel membrane utilizing a ceramic base and biochar, which effectively breaks down the harmful substances in water and shows high resilience to clogging. Das et al.[26] utilized Biochar as a lightweight, cost-effective, and sustainable composite additive, surpassing natural fillers like wood powder in mechanical properties, thermal stability, and decay resistance. Uram et al.[27] explain how to make biochar-modified rigid polyurethane foams for thermal insulation. Biochar was added to polyurethane systems at up to 20% concentration, leading to prolonged foam cells and reduced cross-sectional area. The foams reduced perceived densities by 20% compared to unfilled systems, while retaining a thermal conductivity of 25 mW/mK. This enhanced the foam's geometric and thermal resilience. Alnaser et al.[6] utilized biochar with weight percentages of 0, 2.5, 5, 7.5, and 10% as reinforcement in the aluminum matrix and exhibited enhanced corrosion resistance and mechanical properties. The mechanical strength and hardness of the 7.5 wt.% biochar-reinforced aluminum composite increased by 8.83% and 15.15%, respectively. Corrosion rates dropped by 73% in the 10 wt.% biochar composites, revealing their promise as robust, environmentally friendly materials. Jannet et al.[28] investigated biochar as reinforcement in aluminum metal matrix composites (AMMCs) using the stir-casting process. The addition of biochar at 2.5%, 5%, and 7.5 weight percent increased the material's tensile strength by 18% and its hardness and resistance to wear. These findings highlight biochar's potential as a long-term, sustainable reinforcement for high-performance AMMCs. Parveen et al.[29] investigated biochar-reinforced aluminum metal matrix composites (AAMCs) for improved mechanical and thermal qualities such as hardness, wear resistance, and thermal conductivity. The work used an L27 Taguchi Design of Experiments to improve machining settings on Al5083 alloy with 4%, 8%, and 12% biochar reinforcement generated via stir casting. A cutting speed of 1050 rpm, a feed rate of 60 mm, and a depth of cut of 0.75 mm were ideal, demonstrating the promise of biochar as a high-performance, sustainable engineering material.

In our previous study, we optimized aluminum foam properties by varying the blowing agent ($CaCO_3$) and thickening agent (Al_2O_3) concentrations. The composition AF02 (3% $CaCO_3$, 1% Al_2O_3) showed the best mechanical properties, including high compressive offset stress and energy absorption capacity. However, it also exhibited moderate corrosion resistance and wear performance. The higher $CaCO_3$ content improved strength and microhardness but introduced brittleness, which could impact durability under cyclic loading or harsh conditions. Additionally, AF02's corrosion resistance was lower than AF03 (2% $CaCO_3$, 2% Al_2O_3), which had better pore distribution and fewer oxidation-prone compounds. According to the literature review, biochar was previously utilized to reinforce a variety of materials, including metals, polymers, and soils. Despite growing interest in reinforcing metallic foams with sustainable materials, there remains a significant gap in the literature regarding the use of biochar as a reinforcing agent. This study presents, for the first time, the successful integration of biochar derived from Conocarpus into closed-cell aluminum foams via the liquid metallurgy

technique. The incorporation of this eco-friendly reinforcement unveils a novel trade-off, enhanced corrosion resistance accompanied by a moderate compromise in mechanical strength. By systematically examining the influence of Conocarpus-based biochar on both the mechanical and electrochemical properties of aluminum foams, this research introduces a new approach toward developing lightweight, corrosion-resistant materials with tailored performance. The overarching goal is to optimize the dual functionality of aluminum foams by leveraging the unique characteristics of biochar reinforcement. Unlike traditional materials such as ceramic particles and carbon nanotubes, biochar has distinct properties that make it an attractive long-term reinforcing solution. In this paper, biochar will be individually added as a reinforcement to fabricate aluminum foam samples. Biochar will be incorporated at volume percentages of 1%, 2%, 3%, and 4%. The selection of these reinforcement materials will be based on optimizing the composition identified in our previous study, which is AF02 (3% $CaCO_3$, 1% Al_2O_3). The analysis will focus on assessing compressive stress and energy absorption across four different biochar-reinforced aluminum foam compositions and compare it with our previous studies' optimized composition AF02 (3% $CaCO_3$, 1% Al_2O_3). Additionally, macroscopic analysis will be utilized to characterize the aluminum foam. Furthermore, electrochemical characterization will be conducted to evaluate metal corrosion rates during the corrosion process of solid aluminum foams. Finally, micro Vickers hardness will be measured to determine foam hardness. At the same time, tribological characteristics will be evaluated through specific wear rate analysis using a reciprocating tribological setup.

Material & methods

Raw materials

The primary raw source for aluminum foam is 99.5% pure aluminum. Its elemental makeup, as studied using SpectroMaxx, is shown in Table 1. We obtained this raw material from a Riyadh, Saudi Arabia-based manufacturing firm masdar. Biochar, which is utilized for reinforcement, has been produced in our laboratory as part of another project focused on the production of biofuels from agricultural waste. Lobe Chemie (Mumbai, India) produces Calcium Carbonate ($CaCO_3$) Extra Pure (Article# 02461), a 98% pure foaming agent with particle sizes ranging from 6 to 8 µm. Aztron Technologies (Minnesota, USA) produces aluminum oxide (Al_2O_3) with a high purity of 99.7%. An average particle size of 5 µm effectively stabilizes and thickens molten liquids, increasing their viscosity.

Biochar preparation

Biochar is produced through pyrolysis, a process where biomass is thermally decomposed in the absence of oxygen, preventing combustion and creating a carbon-rich material. In this study, biochar will be prepared from the stem of the Conocarpus plant. The stems will first be cut into small pieces and dried in an oven at 60 °C for 24 hours to remove moisture. Pyrolysis will then be carried out in a tube furnace as shown in Fig. 1, where the dried plant material will be heated to 500 °C for three hours under a nitrogen atmosphere, ensuring complete conversion to biochar. For additional refinement, the resultant charred biomass will be processed into powder using a ball mill with a planetary design (FRITSCH GmbH, USA) to accomplish ultra-fine grinding. A 10:1 ball-to-powder ratio will be used in this procedure, and stainless-steel grinding balls will rotate for 12 hours at 300 rpm.

Foam fabrication

The specimens for further investigation were manufactured under normal air conditions using the blowing agent technique and the liquid metallurgy approach. Aluminum strips from a large aluminum sheet are first placed in a graphite crucible to begin the process. The aluminum strips are then placed in a tabletop furnace and melted at 680 °C. The next step involves adding Al_2O_3 to the molten aluminum and thoroughly mixing it using a mixing head connected to a Bosch PSB 500 RE drill. The drill operates at a constant speed of 1400 rpm, and the mixing process is carried out for 60 seconds. The drill machine's speed was kept at 1400 RPM using a variable voltage controller and a digital tachometer. This stirring operation guarantees that Al_2O_3 is evenly dispersed throughout the aluminum melt, increasing its viscosity. After mixing the alumina, the next step is to add reinforcement, which we have in the form of biochar.

After adding the biochar, thoroughly mix it using a mixing head linked to a Bosch PSB 500 RE drill that is operating at a constant 1400 rpm for 60 seconds. Thorough mixing ensures that the biochar is properly dispersed throughout the melt. After mixing the reinforcement, our melt is ready for the next step, which is to add the blowing agent. The furnace temperature is raised to 770 °C and left to stabilize. Once the furnace has reached this temperature, the next step is to introduce a foaming agent into the aluminum matrix. This is accomplished by incorporating a preset proportion of $CaCO_3$ into the melt. The liquid is then remixed with the mixing head at a constant speed of 1400 rpm for 30 seconds to achieve complete and homogeneous $CaCO_3$ integration inside the melt. To allow for complete foaming, the crucible containing the mixture is placed in the furnace for between sixty seconds and ninety seconds. After being carefully withdrawn from the furnace, the crucible is allowed to cool in the surrounding environment. Finally, the aluminum foam contained within the crucible is carefully removed. In all foam composition production runs, the temperature, stirring time, and stirring speed were consistent. Based on our experience, this time and speed are appropriate for mixing. The mixing head is made

Elements	Fe	Si	Ti	Mn	Na	Ni	Zn	Mg	Cu	Al
Wt.%	0.3524	0.0564	0.0150	0.0035	0.0025	0.0024	0.0022	0.0018	0.0007	Balance

Table 1. Chemical composition of aluminum.

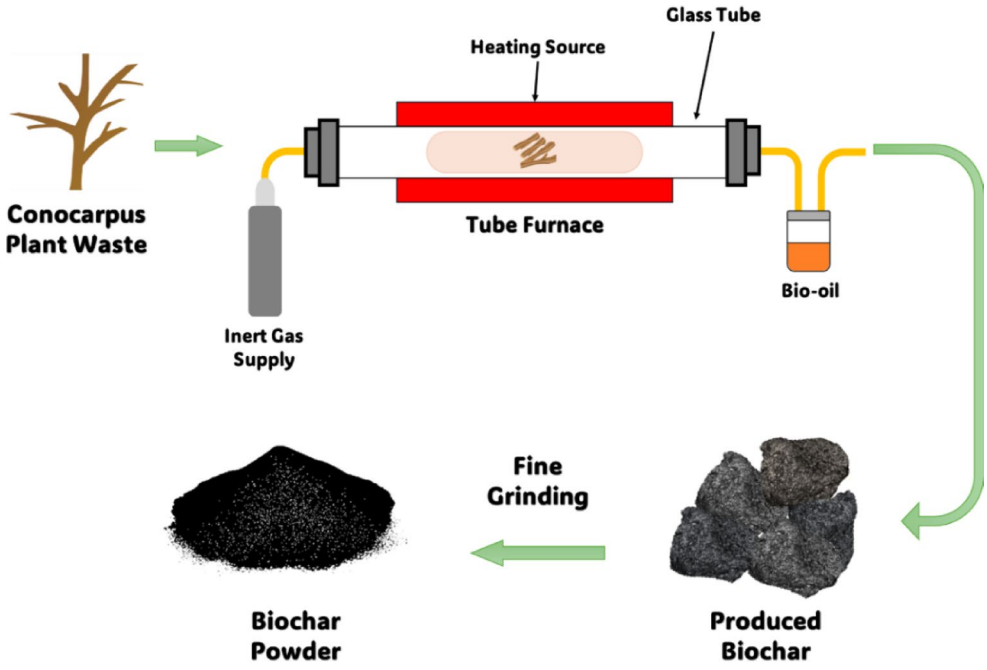

Fig. 1. Schematic diagram of the manufacturing process of biochar.

of steel, which does not affect the chemical composition of the aluminum melt. Figure 2 displays a schematic representation of the aluminum foam production process using the blowing agent method.

This study builds upon our prior investigation into the mechanical behavior of aluminum foam systems, wherein varying proportions of Al_2O_3 and $CaCO_3$ were systematically examined. Among the tested formulations, the composition designated as AF02 (3 wt.% $CaCO_3$ and 1 wt.% Al_2O_3) exhibited superior mechanical performance, as evidenced by its enhanced compressive strength, quasi-elastic gradient, and energy absorption capacity. Owing to its optimized balance of ceramic reinforcement and foaming agent, AF02 has been selected as the baseline matrix for the current phase of the study. In this work, biochar is introduced as an additional reinforcement in varying concentrations (1–4 wt.%) to evaluate its effect on the mechanical and electrochemical properties of the aluminum foam. Table 2 summarizes the optimized AF02 composition and lists the new biochar-reinforced formulations with their corresponding sample IDs, which serve as key reference points throughout this investigation.

Specimen preparation

Concerning their cellular structure, metallic foams require special handling and testing. The size of the specimens affects their apparent modulus and strength; thus, they must be adequately large, at least seven cell diameters in each dimension. The preparation of the surface is critical, and samples cut using diamond cutting or electric discharge techniques show identical properties[18,20,30]. To reduce the destruction of cell structures during sample preparation, we used diamond-cutting equipment, the IsoMet™ Low-Speed Saw, in our study. After manufacturing, three separate specimens were retrieved from every biochar-reinforced aluminum foam composition, and every sample exhibited 15 mm × 15 mm, as shown in Fig. 3. The samples were finally ready for mechanical and electrochemical investigation.

Characterization of foam

Morphology & XRD

The samples were polished on emery paper and then inspected under a Buehler Stereo-zoom optical Microscope to determine their microstructure. This enabled the examination of cell morphology. Images of each composition were obtained employing a consistent source, with a scale for measurement included for reliable measurements, as shown in Fig. 4. We used this scale to establish the scale in the ImageJ program by measuring lengths in pixels/mm. ImageJ was then used to measure the pore diameters. We increased picture contrast by 1.2% and converted photos to binary format[31], allowing for distinct contrast between pores and solid sections, as seen in Fig. 5a. We methodically drew many lines from end to end, zooming in on specific pores, to assess their average size. Given the varied geometries of pores, this technique ensured exact readings, as illustrated in Fig. 5b. We used this procedure to calculate an average pore size for each specimen, using at least eighty pores from a single sample. X-ray diffraction (XRD) tests were performed on all produced materials using a Bruker D8 Discover diffractometer with Cu Kα radiation (1.5418 Å).

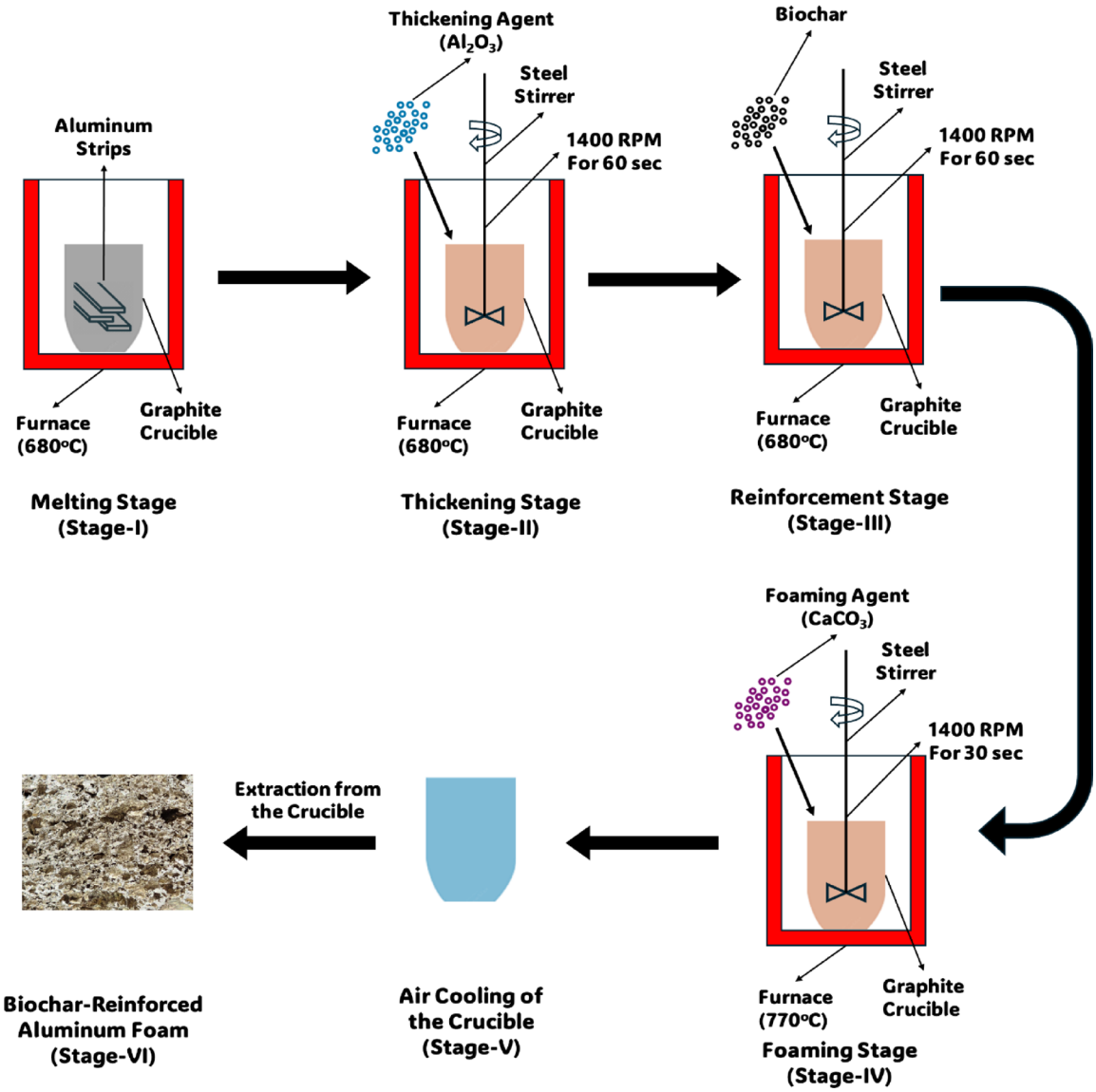

Fig. 2. Schematic of biochar-reinforced aluminum foam fabrication using $CaCO_3$ blowing agent, illustrating mixing, melting, foaming, and solidification stages.

Sr #	Compositions				Sample ID
	% $CaCO_3$	% Al_2O_3	% Biochar	% Al	
1	3	1	–	Balance	AF02
2	3	1	1	Balance	AFB01
3	3	1	2	Balance	AFB02
4	3	1	3	Balance	AFB03
5	3	1	4	Balance	AFB04

Table 2. Composition and their corresponding sample IDs.

SEM and EDS analysis

The SEM investigation was carried out using a JSM-7600F FE-SEM (JEOL, Japan) for two different reasons: (i) to examine high-resolution pictures of particle morphology and grain structures by SEM imaging, and (ii) to conduct an empirical compositional analysis using EDS. To prevent sample charging and improve picture quality, conductive tape was used to connect each sample to the holder. Backscattered electron imaging and EDS analysis also helped to understand the distribution of particles and elemental composition in the samples.

Fig. 3. Biochar-reinforced aluminum foam sample after cutting with a diamond cutter.

Fig. 4. AFB03 biochar-reinforced aluminum foam (3% biochar), shown with measuring scale for size reference.

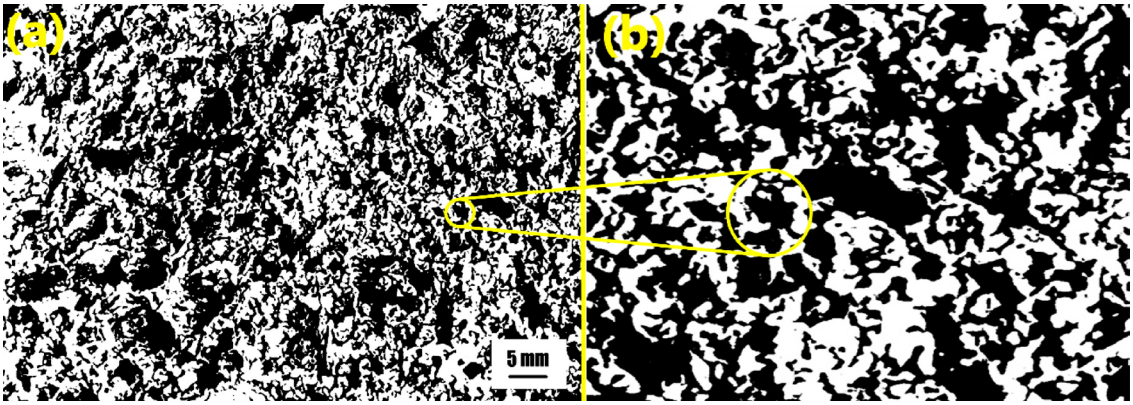

Fig. 5. (**a**) Binary image of AFB02 foam showing pore structure (left), (**b**) Zoomed-in view with pore size measured using reference lines (right).

Density

Density was evaluated by weighing and measuring three separate specimens from each combination. Subsequently, the calculated density was used to determine the relative density and porosity of each chemical composition. Eqs. (1), (2) and (3) were used to calculate the density, relative density, and percentage porosity of the created biochar-reinforced aluminum foam.

Equation (1) Density of biochar-reinforced aluminum foam

$$\rho = \frac{m}{V} \tag{1}$$

Equation (2) Relative density of biochar-reinforced aluminum foam

$$\rho_{relative} = \frac{\rho_{foam}}{\rho_{material}} \tag{2}$$

Equation (3) % porosity of biochar-reinforced aluminum foam.

$$\%P = \left(1 - \frac{\rho_{foam}}{\rho_{material}}\right) \times 100\% \tag{3}$$

Compressive behavior

We performed unidirectional compression experiments under room temperature settings utilizing an INTRON 5984 universal testing instrument at a strain rate of 10^{-3} sec^{-1} to evaluate compressive characteristics. To assure credibility, each foam composition was tested using three samples. The preparation of the sample included meticulous flatness using a diamond cutter machine, followed by placing on the flat platens of the testing equipment, which were oriented perpendicular to the load direction. Before testing, the inner surfaces of the UTM platens were greased with graphite grease to eliminate friction and possibly boost the compressive strength by up to 25%[18]. When the specimens achieved 60% compression, the testing stopped.

Stress-strain data were rigorously collected and reviewed during the experiment to thoroughly investigate the compressive characteristics of metallic foams. These characteristics were evaluated based on the ISO 13314:2011 guidelines[32], It offers a framework for investigating the behavior and features of metal foams and cellular metallic materials. The plateau stress is defined as the average stress recorded within the compressive strain range of 20 to 40%. The quasi-elastic gradient corresponds to the slope of the compressive stress-strain curve's first linear deformation area. The compressive offset stress is the stress level recorded at 0.2% plastic compressive strain. These criteria are crucial for determining the mechanical behavior of materials and are defined in applicable standards. These phrases are crucial parameters for understanding the mechanical behavior of metallic foams under compression[33–35].

Furthermore, energy absorption is an important attribute of metallic foam that is used in a variety of technical applications. It has a direct relationship with the area beneath the stress-strain curve. Metallic foams have a unique plateau stage after elastic yielding during uniaxial compression. As a result, the energy absorption capacity (W) is measurable by integrating stress from the starting strain of 0% up to the densification strain, which is generally approximately 60% strain, on the stress-strain curve, as shown in Eq. (4) allowing a complete study in engineering research[36,37]:

Equation (4) Energy absorption capacity of biochar-reinforced aluminum foam

$$W = \frac{1}{100}\int_{0}^{\varepsilon_0} \sigma \cdot d\varepsilon \tag{4}$$

Electrochemical characterization

Using linear polarization, electrochemical characterization was performed to determine the degree of corrosion of each combination. These studies were carried out with a 0.5 M industrial NaCl solution. The research investigations were carried out in a cell equipped with three electrodes: Ag/AgCl as the electrode used for reference (RE), platinum foil as a counter electrode (CE), and biochar-reinforced aluminum foam compositions as the working electrodes. To prepare for electrochemical assessments, these specimens have been sliced into cubes with a 1 cm^2 revealed corrosion area using a diamond cutter. Afterward, emery paper was used to polish the surfaces.

Linear polarization was carried out utilizing an Autolab system (PGSTAT20, Metrohm, Netherlands), using a 30-minute stabilization time frame before starting every test. The linear polarization experiment included adjusting the voltage from -500 mV to +500 mV at a scanning rate of 0.00166 V/s, relative to the open circuit potential (OCP) beside the reference electrode (RE)[38,39]. Thus, using Eq. (5), we can determine the corrosion rate of biochar-reinforced aluminum foams in NaCl solutions:

Equation (5) Corrosion rate of biochar-reinforced aluminum foam.

$$C.R. = 0.129 \times \frac{a \times i_{corr}}{n \times \rho} \tag{5}$$

where 0.129 is the coefficient of proportionality used to calculate the rate of corrosion in mils per year (mpy); In this equation, "*a*" represents aluminum's atomic weight (26.51 g/mol), i_{corr} is corrosion current density (μA/

cm^2), n is the number of moles (3 mol), and ρ is the density of aluminum (2.65 g/cm^3). All the variables in the equation above are available in the literature, except the current density, which is calculated using Eq. (6) from the corrosion current density $i_{corr,}$ and the contact area of the working electrode.

Equation (6) Current density of biochar-reinforced aluminum foam.

$$i = \frac{i_{corr}}{A} \tag{6}$$

The corrosion current density (i_{corr}) was calculated by projecting the anodic and cathodic Tafel lines to the linearized current area.

Reciprocating tribology tests

The Bruker tribometer (UNMT-1 L) was utilized for carrying out linear reciprocating tribology tests under dry circumstances at room temperature using a pin-on-disc configuration. During testing, the sample was firmly secured perpendicular to the stainless steel disk with a screw arrangement within the sample container. Figure 6 shows a schematic for a reciprocating tribology test rig. For 10 minutes, a 15N force was applied across a sliding distance of 12 meters. The test entailed maintaining an uninterrupted back-and-forth linear slide motion of 30 mm on the disc in each direction, with a consistent sliding rate of 20 mm/sec throughout the testing. The specimens' weights were determined beforehand and following the test using an electronic weighing device with an accuracy of up to four decimals. Eq. (7) was used to calculate the specific wear rate and coefficient of friction for each specimen, as shown below[40–43].

Equation (7) Specific wear rate for biochar-reinforced aluminum foam.

$$SWR = \frac{m_1 - m_2}{\rho \times l \times f_n} \tag{7}$$

where m_1 in mg indicates the initial measurement weight of the sample, m_2 in mg reflects the final weight of the sample after tests, ρ is the density of the foam in mg/mm^3, l indicates sliding distance in m, and f_n designates the applied force in N.

Microhardness measurement

The Zwick Roell indentec Vickers micro-hardness machine was used to investigate biochar-reinforced aluminum foam microhardness properties. The applied load was 50 gmf, with a dwell time of 10 seconds. The indentation measuring sites were carefully positioned at twice the size of the indentation itself. Following these accurate measurements, the average hardness was estimated methodically by aggregating data from ten different points collected across the specimen.

Results & discussions

Biochar characterization

As seen in Fig. 7, SEM images taken at different magnifications demonstrate that the granulated biochar has a high degree of porosity, with an average pore size of 4 to 14 microns and an overall porosity of around 55%. According

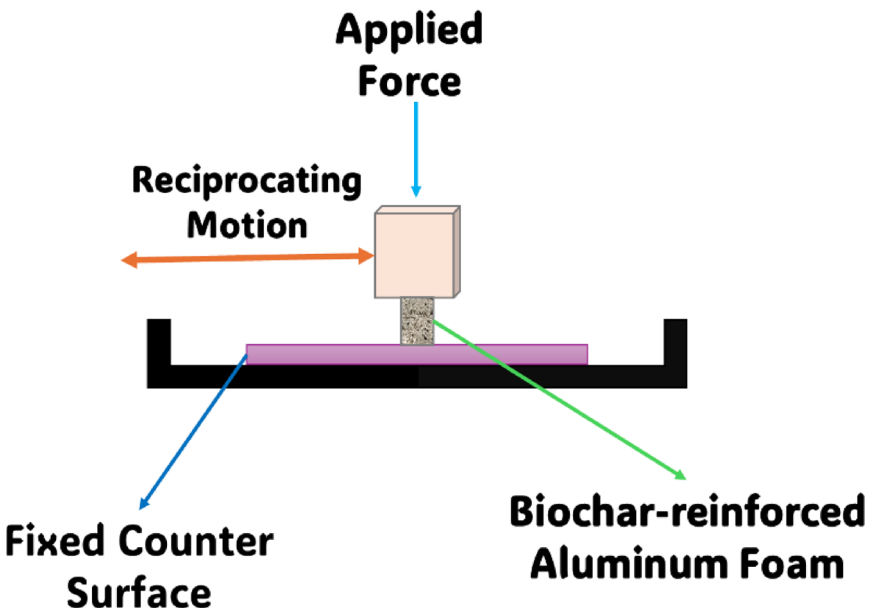

Fig. 6. Reciprocating tribology test setup for biochar-reinforced aluminum foam showing sample, load direction, and sliding motion.

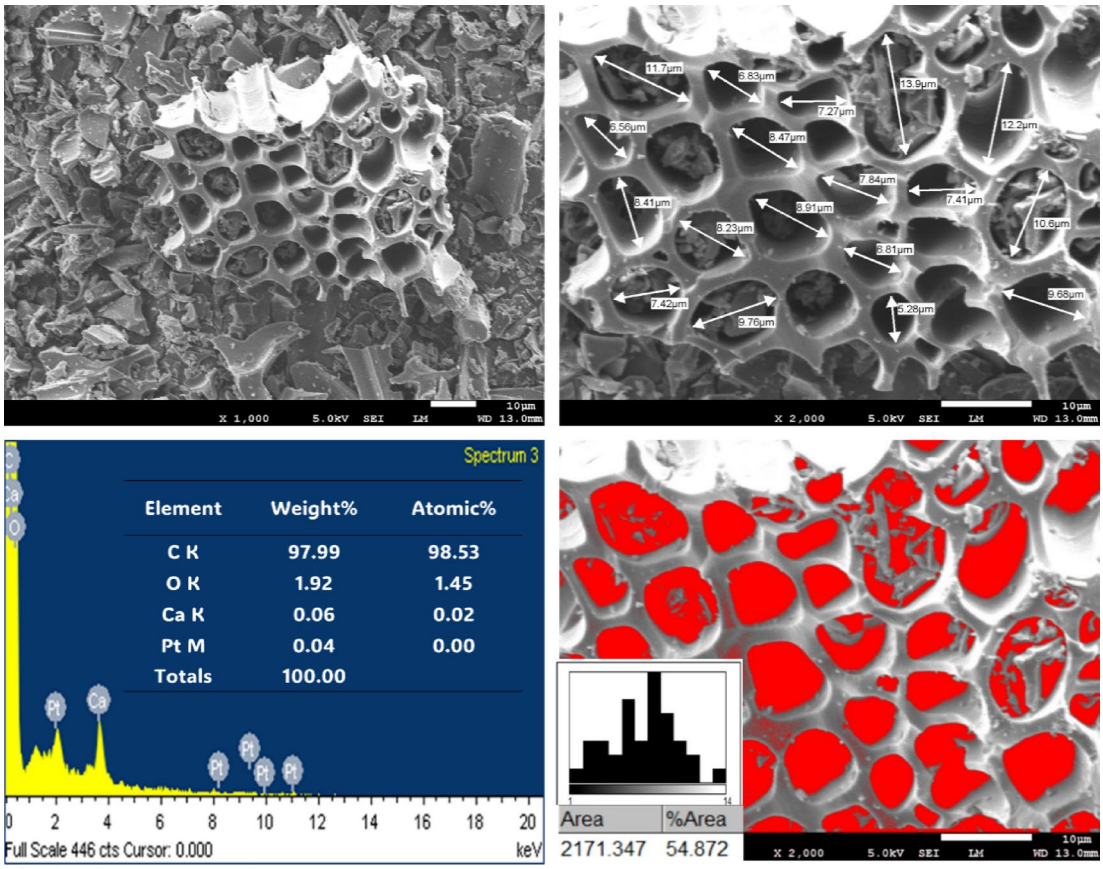

Fig. 7. SEM & EDS analysis of produced biochar.

to an investigation using energy-dispersive X-ray spectroscopy (EDS), the biochar is mostly made up of carbon and oxygen, with trace levels of calcium. The platinum observed in the EDS spectrum is from a platinum coating that was applied to increase surface conductivity, reduce charging effects, and ensure good SEM pictures. The porosity in the biochar structure provides pathways that enhance the total surface area, improving the contact surfaces between the matrix and filler. This has a significant impact on the material's mechanical characteristics. The ultra-fine powder produced by this technique is expected to substantially enhance the characteristics of biochar, making it an excellent choice for reinforcement in aluminum metal foam applications.

Biochar-reinforced aluminum foam morphology &XRD

Figure 8 shows the microstructure of cross-sections from different biochar-reinforced aluminum foam compositions. In composition AFB01, the cell size is more uniform and evenly distributed compared to the others. As the biochar content increases, the pore size becomes larger and more irregular, reducing the uniformity. In composition AFB04, some cells collapse due to melt drainage, leading to elongated cells that are aligned perpendicular to the foam direction. The cell walls in this composition are ruptured and thinner, while the thickness of the cell struts increases. Table 3 presents the average pore sizes for five different compositions, comparing AF02 from Phase-I with four biochar-reinforced aluminum foam compositions. This table highlights the impact of biochar concentration on pore size. AFB01 (1% biochar) has the smallest average pore size, while increasing the biochar content up to 4%, as in AFB04, results in the largest pore size. As shown in Fig. 7 the laboratory-produced biochar has a porous structure. When mixed with aluminum foam, it increases the pore size of the optimized foam from Phase-I, from 1.881 mm to 2.077 mm.

Figure 9, is a histogram showing the average pore size distribution of biochar-reinforced aluminum foam samples. The average pore diameters for different compositions are as follows: AFB01 ranges from 0.195 to 7.894 mm, AFB02 from 0.637 to 10.308 mm, AFB03 from 0.547 to 10.247 mm, and AFB04 from 0.368 to 9.952 mm. Phase-I AF02 ranges from 0.38 to 5.764 mm. The results clearly show a consistent trend of increasing pore size as the biochar content, known for its porous nature, rises from 1% to 4% in the optimized composition (3% $CaCO_3$ and 1% Al_2O_3) from Phase-I.

Biochar-reinforced aluminum foam SEM and EDS analysis

The SEM images of biochar-reinforced aluminum foam reveal key structural details. In Fig. 10, the aluminum foam displays a closed-cell structure with clearly defined cell walls, which contributes to the material's lightweight properties and mechanical strength. These closed cells, fully enclosed by cell walls, enhance energy absorption, making the foam suitable for applications in fields like automotive and aerospace. Figure 11 highlights the

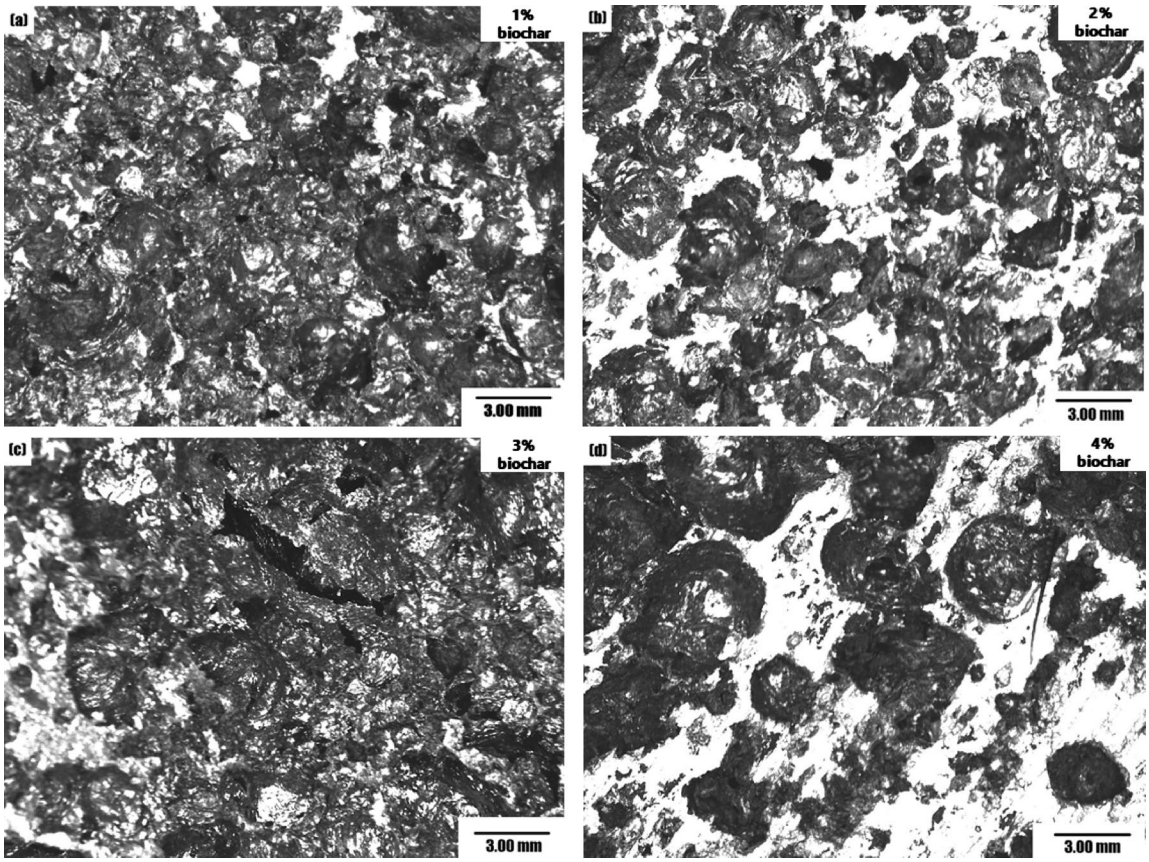

Fig. 8. Microstructure of biochar reinforced aluminum foam compositions, (**a**) AFB01, (**b**)AFB02, (**c**)AFB03, (**d**)AFB04.

Compositions	Average pore size (mm)
AF02 (optimized from phase-I)	1.881 ± 0.833
AFB01	2.077 ± 1.812
AFB02	2.941 ± 1.734
AFB03	3.151 ± 2.263
AFB04	2.649 ± 2.129

Table 3. Biochar-reinforced aluminum foam average pore size.

distribution of biochar particles on the foam's surface. The biochar particles are irregularly shaped and vary in size, indicating good dispersion, which can improve the foam's thermal stability, electrical conductivity, and corrosion resistance. The surface texture surrounding the biochar also suggests a rough morphology, potentially aiding in bonding between the biochar and aluminum matrix. Together, these features illustrate an optimized microstructure where biochar reinforcement may significantly enhance the foam's performance attributes. As the biochar content increases, the pore size continues to grow, which can be seen in Fig. 12.

Figure 13 shows the XRD analysis of different biochar-reinforced aluminum foam compositions. The initial peaks in each composition indicate the presence of intermetallic compounds, including α-alumina and aluminum, along with small traces of aluminum silicate and calcium silicide. The foaming and thickening agents contribute to the formation of intermetallic compounds like Al-Ca and α-Al. Figure 14 highlights the XRD peaks for the AFB02 composition, as identified by the Xpert High Score program.

The XRD studies of the samples from AFB01 to AFB04 in Fig. 13 displayed differences concerning several factors such as intensities of peaks, their sharpness, broadening, and crystallinity. Sample AFB02 has, in comparison to its counterparts, very sharp and very intense diffraction peaks, notably around the main reflections at 38°, 45°, and 65°, indicating a high degree of crystallization, crystallite size, and very low lattice strain. On the contrary, AFB03 shows broader and less intense diffraction peaks, representing disorder in microstructure with small crystallite size and high internal strain. AFB04 inhibits sharp peaks but with slightly less intensity than AFB02, thereby connoting a high degree of crystallinity. AFB01 is rather intermediate and characterized by moderate peak broadening and structural order. Furthermore, the diffraction peaks of AFB02 are quite well

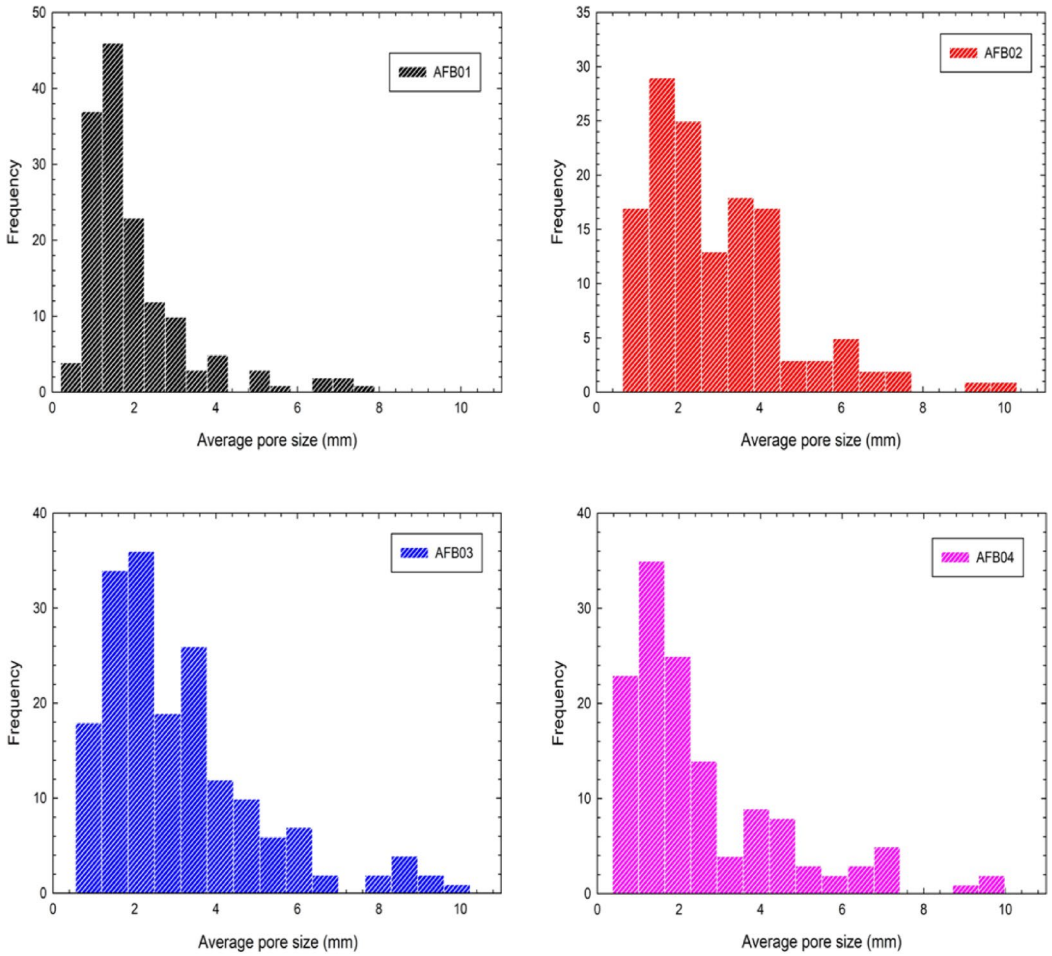

Fig. 9. Pore size distribution of fabricated biochar-reinforced aluminum foams.

separated and clear, which speaks of well-defined phase formation and better crystallographic orientation. This means that AFB02 has a microstructure that is the most refined and well-ordered, whereas AFB03 is somewhat less crystalline and distorted structurally.

Composition AF02 from Phase-I shows that 1% Al_2O_3 improves foam stability by trapping more gas during the decomposition of 3% $CaCO_3$, which enhances the formation of Al-Ca intermetallic compounds. After incorporating biochar into the optimized composition, AFB02 exhibits the highest initial peak among all biochar-reinforced samples. As shown in Fig. 14, AFB02 contains minimal traces of carbon, along with aluminum and alumina, and features intermetallic compounds such as calcium aluminates, aluminum silicates, and calcium silicide. Additionally, the silicon in the pure aluminum used for foam fabrication, combined with carbon from biochar, leads to the formation of silicon carbide in the biochar-reinforced aluminum foam.

Biochar-reinforced aluminum foam density

Table 4 compares the relative density and porosity percentages of various biochar-reinforced aluminum foam samples with the AF02 composition from Phase I. AFB03 shows a higher porosity percentage, indicating a less dense foam structure, while AFB04 exhibits the highest relative density percentage and the lowest porosity among the samples. The table illustrates a trend in relative density and porosity percentages from AFB01 to AFB04: there is a decrease in relative density followed by a significant increase in AFB04. Similarly, the porosity percentage shows an upward trend from AFB01 to AFB03, with a notable decrease observed in AFB04. Figure 15 illustrates the influence of biochar on pore size, relative density, and porosity percentage in biochar-reinforced aluminum foam.

As demonstrated in Fig. 7, biochar itself possesses a porous structure. When integrated into the optimized aluminum foam composition from phase I, biochar enhances the porosity percentage while concurrently decreasing the relative density. This relationship is depicted in Fig. 15, where a high-density foam and a foaming region are evident. However, the addition of 4% biochar leads to the emergence of a failed foaming region due to an excess of biochar. This surplus results in increased pore sizes, and the merging of two or more pores into a single larger cell compromises structural integrity. The larger cells are unable to sustain themselves, ultimately leading to bursting. As a result, the production of foam is significantly reduced, yielding minimal or no foam.

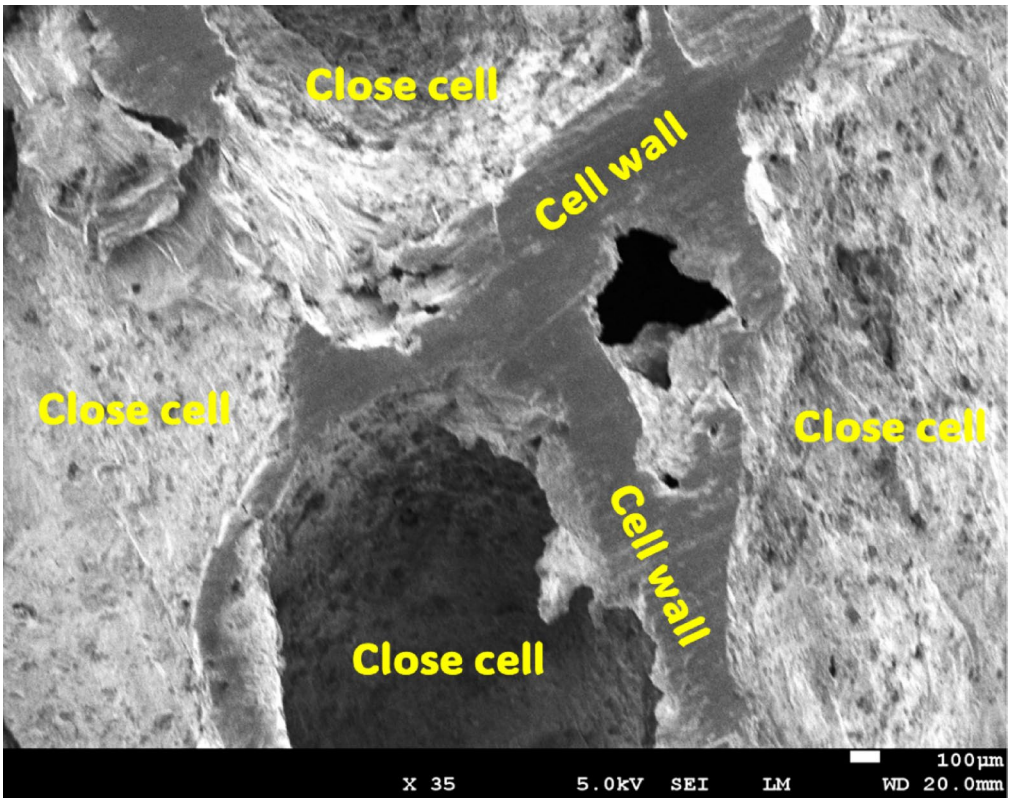

Fig. 10. SEM analysis highlighting the microstructure of closed-cell biochar-reinforced aluminum foam.

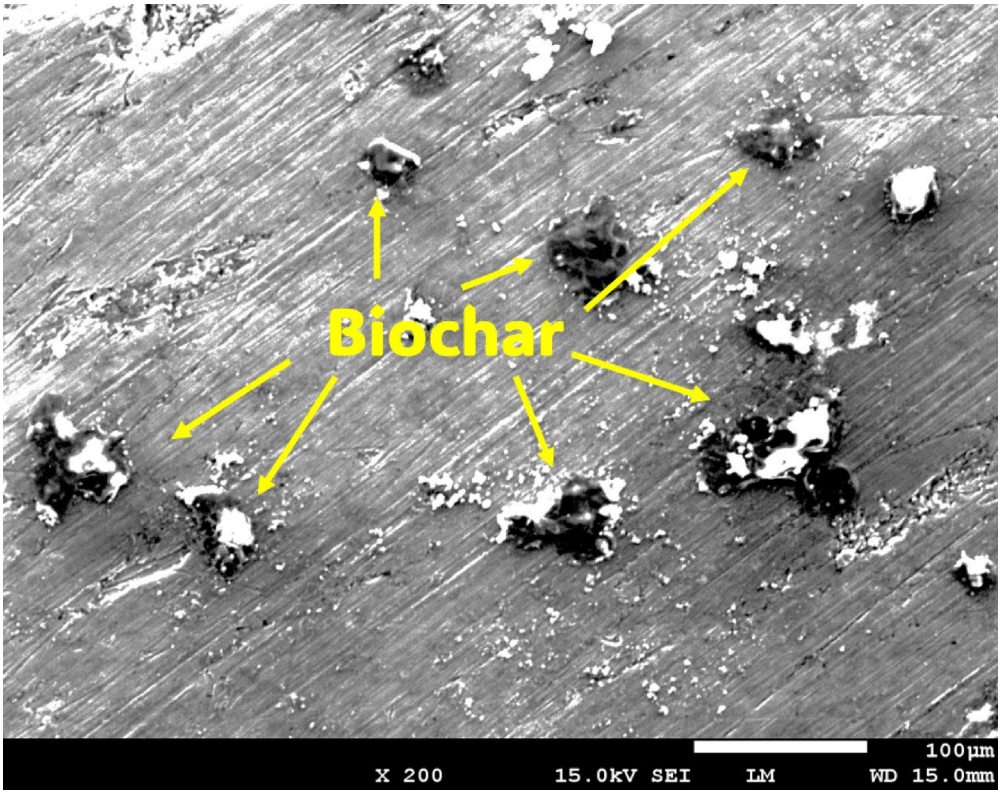

Fig. 11. SEM analysis revealing the distribution of biochar in the reinforced aluminum foam composite.

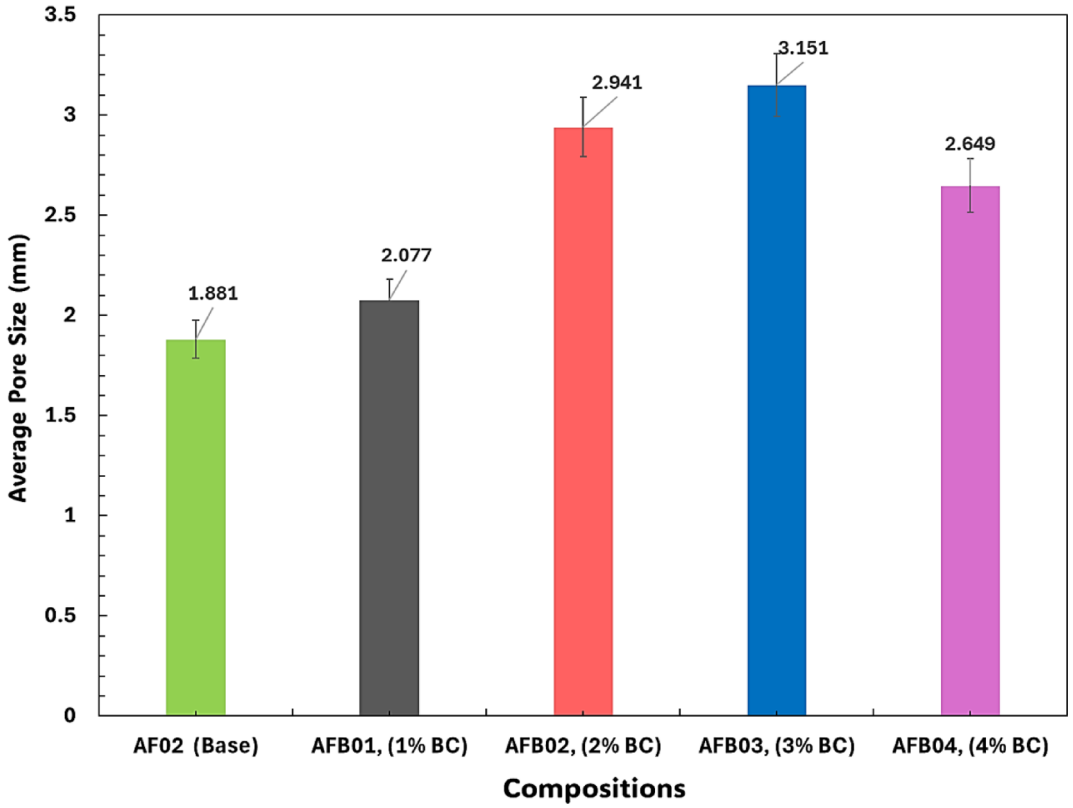

Fig. 12. Biochar-reinforced aluminum foam average pore size.

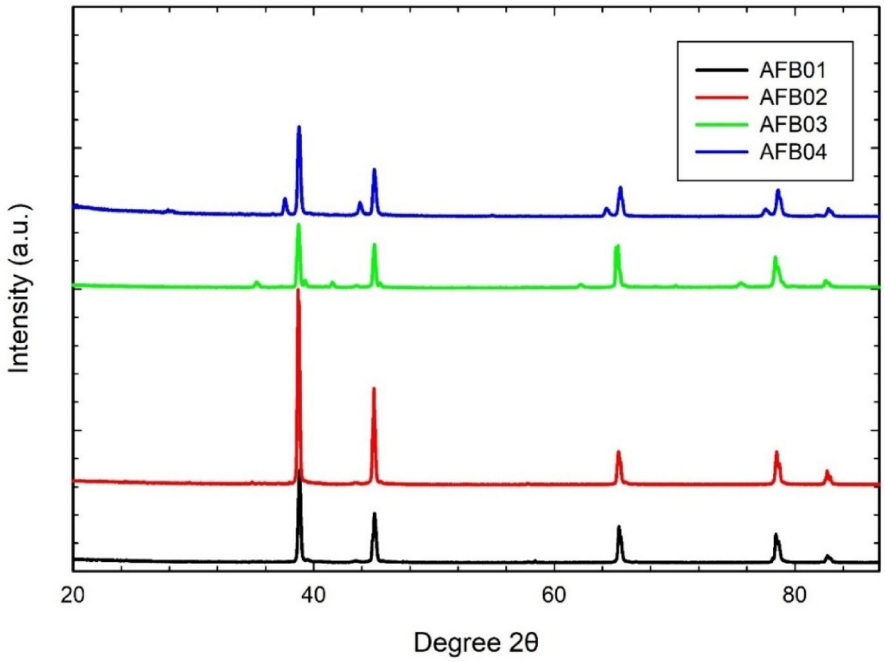

Fig. 13. XRD patterns for biochar-reinforced aluminum foam compositions.

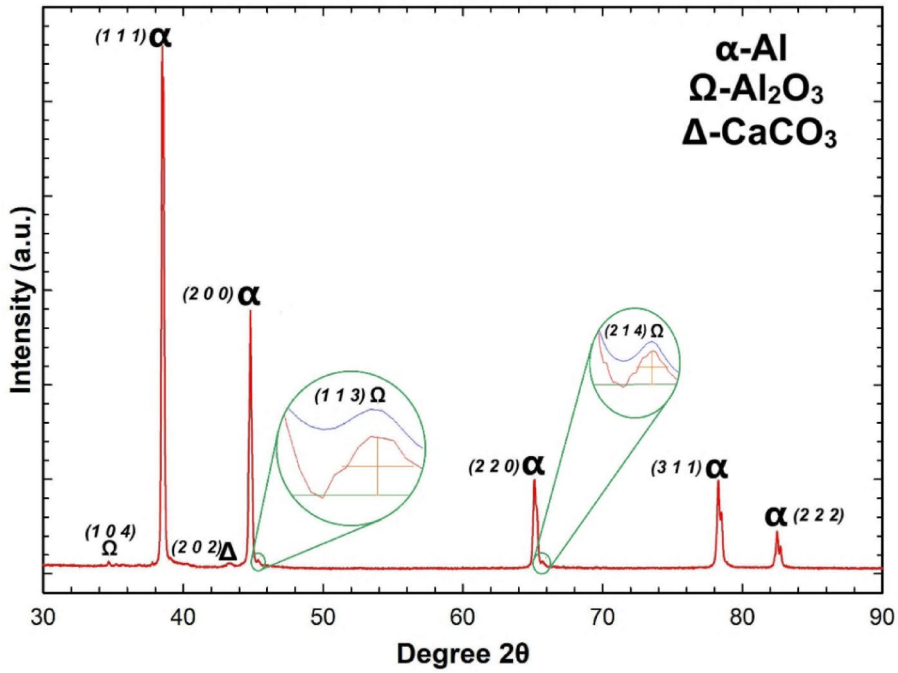

Fig. 14. XRD pattern of AFB02 biochar-reinforced aluminum foam.

Compositions	Relative density% $\left(\rho_f/\rho_m\right)$	Porosity%
AF02 (optimized from phase-I)	21.1 ± 1.19	78.9 ± 1.19
AFB01	17.04 ± 1.31	82.96 ± 1.31
AFB02	13.90 ± 1.61	86.10 ± 1.61
AFB03	13.26 ± 1.63	86.74 ± 1.63
AFB04	30.81 ± 1.69	69.19 ± 1.69

Table 4. Relative density & porosity% of biochar-reinforced aluminum foam.

This phenomenon is characterized by an unexpected increase in relative density and a corresponding decrease in porosity percentage as observed in AFB04 [16].

Biochar-reinforced aluminum foam compression properties

Three major stages are identified by the stress-strain curves shown in Fig. 16, which provide information on the mechanical behavior of foam compositions during uniaxial compression testing: (i) elastic deformation, (ii) plateau area, and (iii) densification stage. A recurring pattern appears in all compositions: there is a linear elastic reaction at first, where stress rises proportionately and the pore walls crack and bend under pressure. The plastic yielding, or plateau, stage occurs when the pore walls fail owing to severe buckling, resulting in consecutive shearing and rupture. Stress progressively increases with strain throughout this period, and more porosity produces a flatter curve. For the lowest porosity, the stress-strain curve seems smooth. Figure 17 shows the zoomed stress-strain up to 60% strain. Nonetheless, the curve exhibits minor fluctuations in the plateau area as the porosity % rises. These variations are produced by the increased number of pores, which makes the foam more unstable during compression, resulting in less smooth and more irregular stress-strain curves. Finally, during the densification step, metallic foam consolidates, resulting in a significant increase in stress as strain increases. The plateau region shows stress increases due to crack initiation at particle-matrix interfaces, such as undecomposed $CaCO_3$, CaO, and Al_2O_3. AF02 from Phase-I, containing 3% $CaCO_3$ and 1% Al_2O_3, shows the highest compressive performance. However, the addition of biochar results in reduced performance from AFB01 to AFB03, due to increased porosity and decreased relative density as the biochar content rises from 1% to 3%. The compression behavior of the AFB03 composition of biochar-reinforced aluminum foams can be seen in further detail in Figure 18, where four distinct stages are shown up to 60% strain at a steady rate of 10^{-3} sec^{-1}.

Table 5 provides a detailed comparison of the compressive properties of biochar-reinforced aluminum foam based on the stress-strain curves. The table compares the optimized composition from Phase-I (AF02) with biochar-reinforced aluminum samples containing 1% to 3% biochar. Under uniaxial compression, the foam's cellular structure undergoes several stages of deformation, including wall bending, collapse, rupture, and densification. These deformations result in lower compressive strain in the biochar-reinforced samples

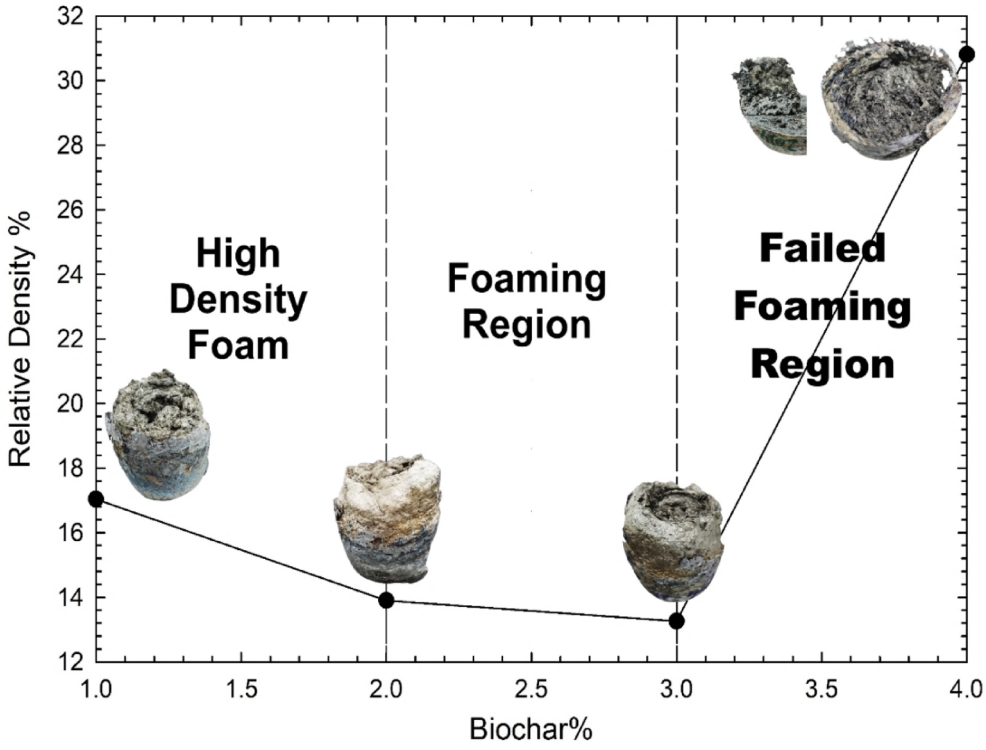

Fig. 15. Graphical representation of the relative density% of reinforced aluminum foam vs. biochar%

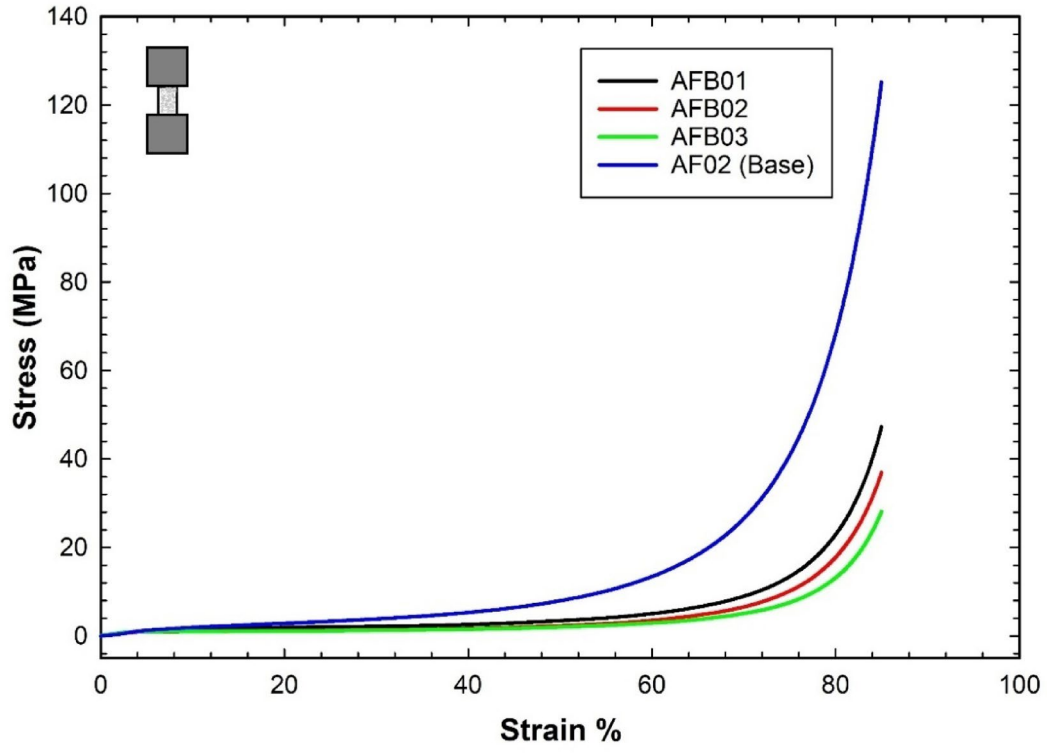

Fig. 16. Stress–strain graph of biochar-reinforced aluminum foams up to 85% strain.

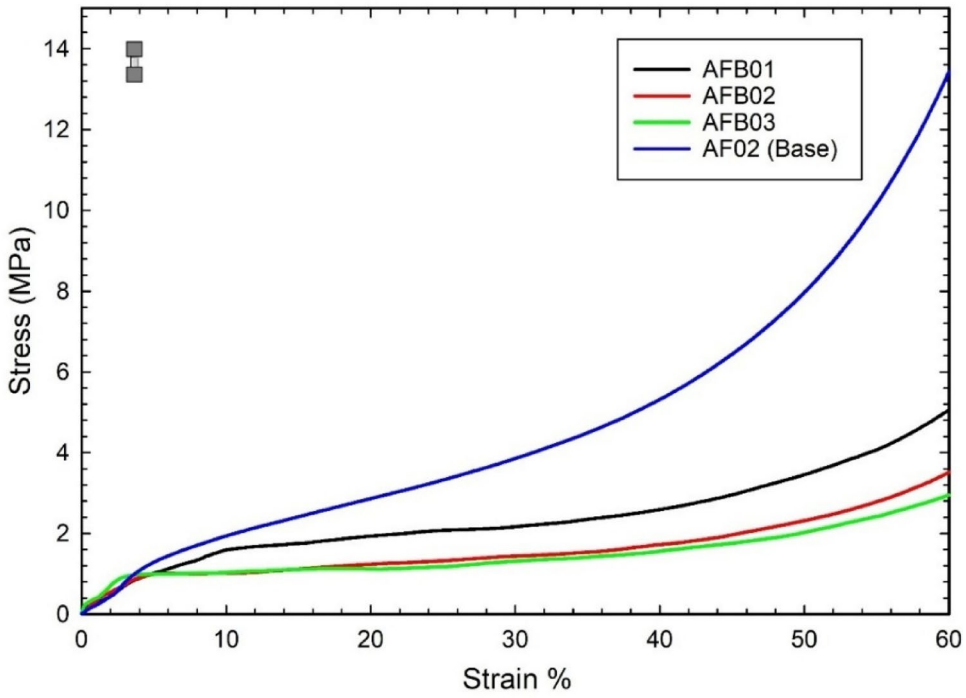

Fig. 17. Stress–strain graph of biochar-reinforced aluminum foams up to 60% strain.

compared to AF02. The biochar-reinforced foams exhibit significantly lower compressive offset stress than AF02 from Phase I. This reduction in performance can be attributed to the microstructural changes induced by the addition of biochar. As the biochar content increases from 1% to 3%, a continuous carbon network forms within the aluminum matrix, altering the foam's internal structure. This network compromises the foam's ability to withstand compressive forces, leading to a decrease in mechanical performance. The formation of the carbon network disrupts the uniform stress distribution throughout the foam, increasing its susceptibility to buckling and failure at lower stress levels. Additionally, the porous nature of biochar further weakens the foam's structural integrity, contributing to a reduction in compressive strength. As a result, compressive properties decline with increasing biochar content, making the biochar-reinforced samples more fragile compared to the optimized AF02 composition. Interestingly, the quasi-elastic gradient shows a downward trend after adding 1% biochar, but this trend reverses after adding 2% and 3% biochar. This improvement may be attributed to the reinforcing effect of the carbon network formed by the increased biochar content.

In Table 6, the data presented in the table highlight the compressive properties of biochar-reinforced aluminum foam, comparing the plateau stress (σ_{pl}) and energy absorption (W) of various compositions. AF02, the optimized composition from Phase-I, exhibits the highest plateau stress at 3.93 MPa, demonstrating superior mechanical performance. This can be attributed to its optimized microstructure, which remains strong and stable under compression. However, as biochar is introduced into the foam matrix (AFB01 to AFB03), the plateau stress progressively decreases. AFB01, with 1% biochar, shows a significant drop to 2.21 MPa (a reduction of 43.7%), and the trend continues with AFB02 and AFB03, which exhibit 1.44 MPa and 1.31 MPa, respectively. The reduction in plateau stress correlates with the increasing biochar content, as biochar's porous nature and the formation of a carbon network within the aluminum matrix weaken the foam's structural integrity, reducing its ability to sustain compressive forces.

As per the literature, increased porosity in metal foams reduces mechanical strength due to pore coalescence and the formation of stress concentrators. Larger, interconnected pores act as weak points, promoting crack initiation and failure. Thinner cell walls further reduce load-bearing capacity, making the structure more susceptible to deformation. Similarly, in this research, as biochar content increased from 1% to 4%, pore size also increased, leading to reduced strength. At 4% biochar, excessive pore coalescence resulted in abnormally large pores and a failed foaming region, confirming the detrimental effect of high porosity on foam integrity[44].

Energy absorption refers to the energy absorbed per unit volume by a specimen when subjected to compression up to a specified strain. The energy absorption capacity is graphically represented as the area under the stress-strain curve. In this study, the trapezoidal approximation method was employed to calculate the energy absorption integral, as detailed in Eq. (4). The energy absorption properties are primarily influenced by the collapse of the pore structure, particularly during the plateau stage of deformation. This aspect is essential for assessing the energy absorption capacity of metallic foams under compressive loading. Similarly, the energy absorption capacity of the foams also declines with the addition of biochar. AF02 absorbs the most energy, with a value of 2.82 MJ/m^3, due to its higher plateau stress and strong cellular structure. In contrast, AFB01, AFB02, and AFB03 exhibit decreasing energy absorption values of 1.42 MJ/m^3, 0.96 MJ/m^3, and 0.88 MJ/m^3, respectively. These reductions, ranging from 49.6% to 68.8% compared to AF02, reflect the diminished ability

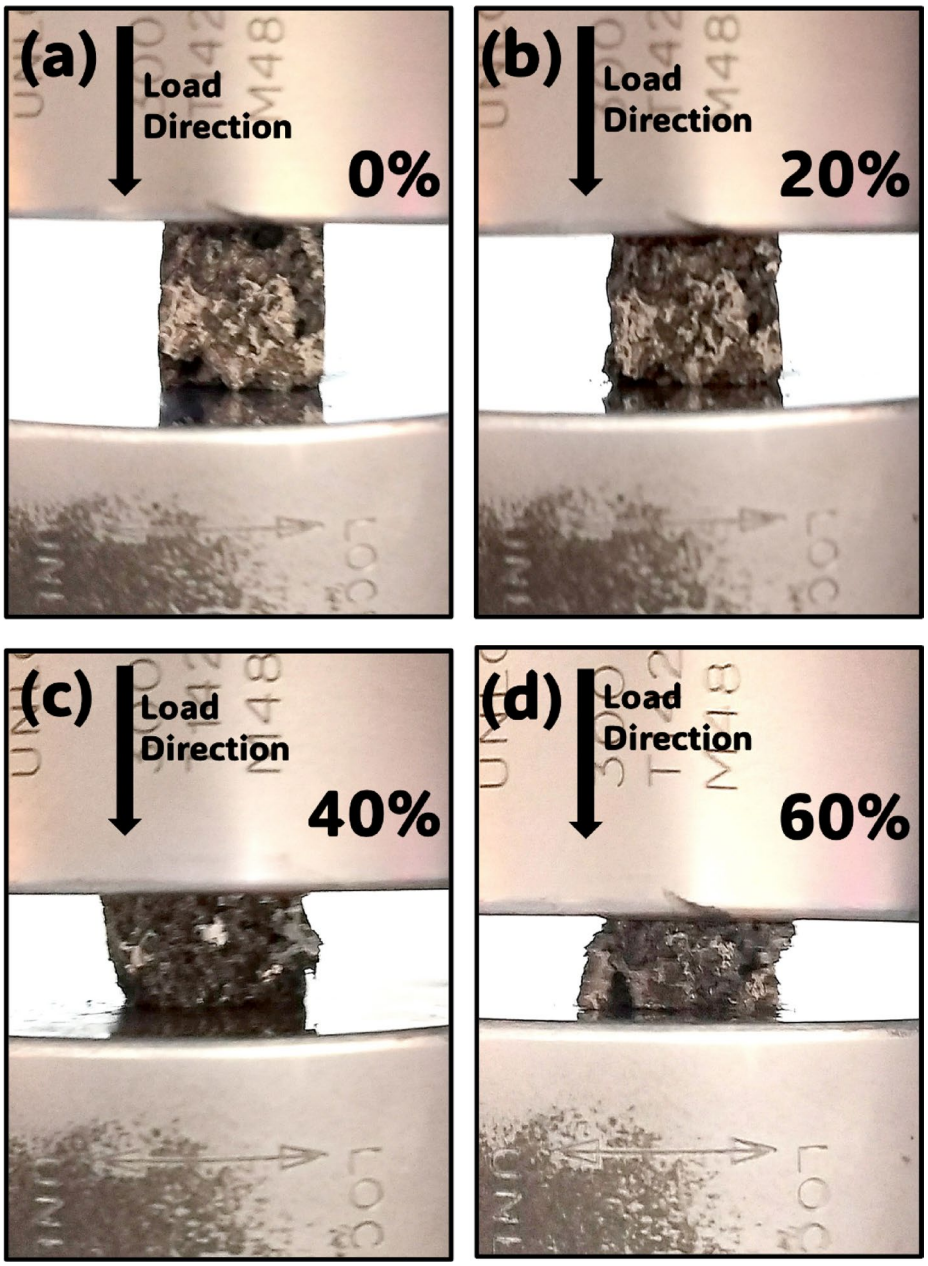

Fig. 18. Four stages of AFB03 composition uniaxial compression test from 0 to 60% densification (arrow direction represents the upper jaw moment).

Compositions	Compressive offset stress (MPa), $\sigma_{0.2}$	Quasi-elastic gradient (MPa)
AF02 (optimized from phase-I)	1.73	21.31
AFB01	1.01	20.78
AFB02	0.94	22.00
AFB03	0.98	24.51

Table 5. Compressive properties of biochar-reinforced aluminum foams.

of the biochar-reinforced foams to absorb mechanical energy efficiently. The increased biochar content results in a more fragile foam structure, limiting its energy absorption capacity during deformation[45,46]. Additionally, the energy absorbed at 50% strain is determined from Fig. 19, where a straight line perpendicular to the x-axis is drawn. The corresponding values are extracted and verified from Table 6, confirming consistency in the data. This table also shows that the energy absorbed at 50% strain is a key parameter in evaluating the ability of

Compositions	Plateau stress, σ_{pl} (MPa)	Energy Absorption, W (MJ/m^3)	Energy absorbed at 50% strain, (MJ/m^3)
AF02 (optimized from phase-I)	3.93	2.82	1.93
AFB01	2.21	1.42	1.04
AFB02	1.44	0.96	0.71
AFB03	1.31	0.88	0.66

Table 6. Plateau stress and energy absorption values of biochar-reinforced aluminum foam.

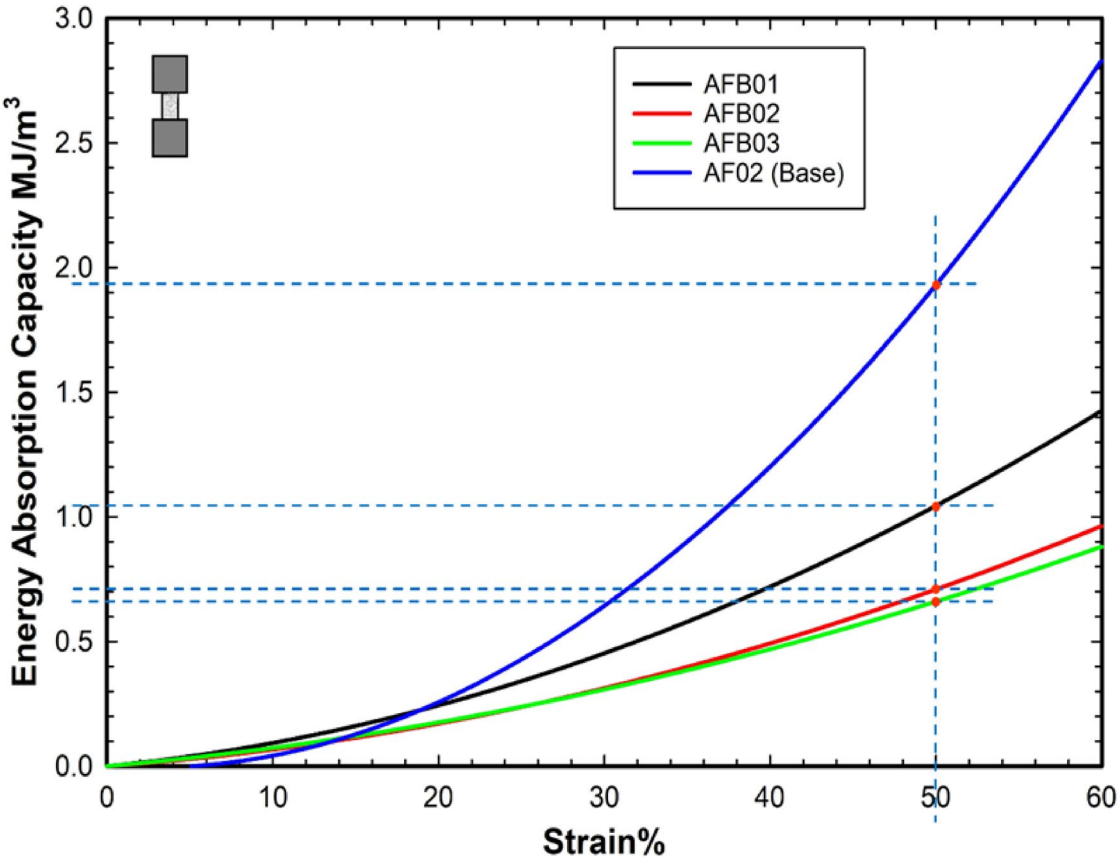

Fig. 19. Energy absorption capacity curves of biochar-reinforced aluminum foams for 50% strain.

aluminum foam to dissipate energy under compression. Commercially pure aluminum foam has an energy absorption capability of around 0.70 MJ/m^3 at 50% strain[47]. Among the tested compositions, AF02 exhibited the highest energy absorption of 1.93 MJ/m^3, indicating its superior ability to withstand deformation while effectively absorbing impact energy. In contrast, the biochar-reinforced samples (AFB01, AFB02 & AFB03) showed a decreasing trend in energy absorption, with AFB01 at 1.04 MJ/m^3, AFB02 at 0.71 MJ/m^3, and AFB03 at 0.66 MJ/m^3. This decline suggests that the incorporation of biochar negatively affects the foam's energy absorption capability, likely due to increased brittleness and the introduction of structural imperfections. The lower energy absorption in biochar-based foams may be attributed to weakened cell walls or inhomogeneous reinforcement distribution, which could lead to stress concentrations and premature failure during deformation. In contrast, the optimized composition of AF02, reinforced with $CaCO_3$ and Al_2O_3, appears to enhance the foam's mechanical performance by providing a more stable and uniform cellular structure.

Overall, the addition of biochar leads to a reduction in both compressive strength and energy absorption, with higher biochar content further degrading the foam's mechanical performance. While biochar may reduce the foam's density, its porous nature and impact on the matrix structure diminish its ability to withstand and absorb compressive forces. Therefore, while biochar-reinforced aluminum foams show potential, their mechanical properties need careful optimization to prevent significant losses in strength and energy absorption compared to the optimized Phase-I composition (AF02). Our work aligns closely with previous studies on closed-cell metal foams. Similar to the AZ31 magnesium alloy foam, Xia et al. found that increasing porosity leads to a sharp decline in energy absorption and compressive strength. In the AZ31 foam, performance dropped significantly between 60% and 75% porosity, which matches our observations where adding biochar increased porosity and reduced strength[48]. In Fig. 20, the energy absorption capacity vs. stress graph for biochar-reinforced aluminum

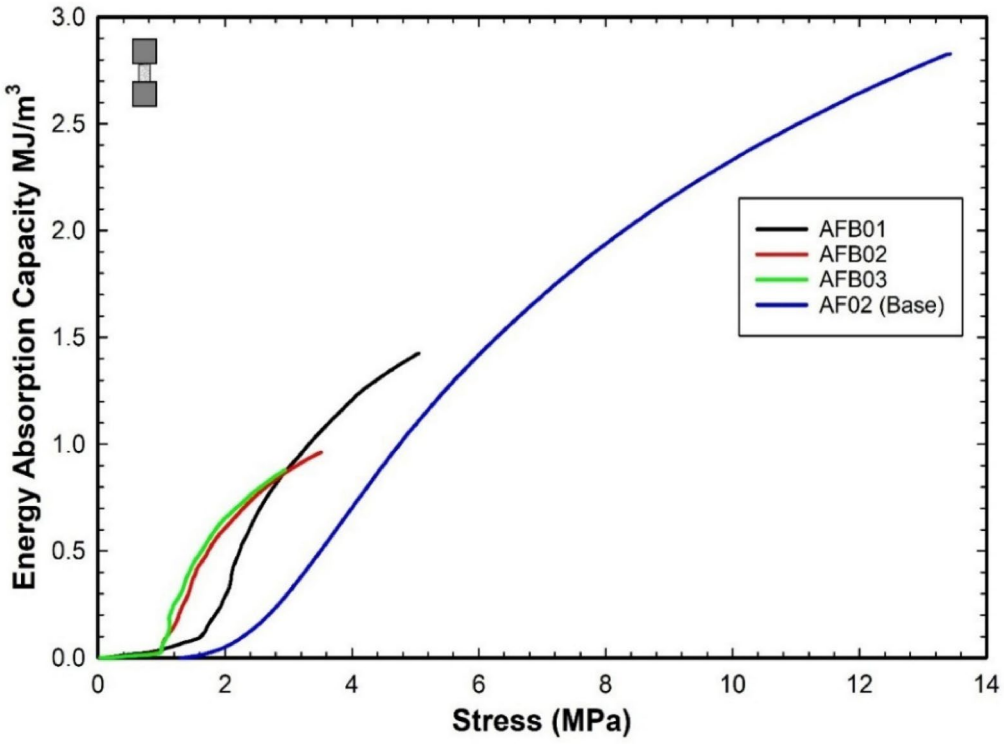

Fig. 20. Energy absorption capacity vs stress graph for biochar reinforced aluminum foam composition at 60% strain.

Compositions	I_{corr}, µA/cm^2	Corrosion rate (mpy)
AF02 (optimized from phase-I)	690.56	2086.04
AFB01	77.83	235.12
AFB02	106.18	320.74
AFB03	191.90	579.70

Table 7. Icorr and corrosion rate of biochar-reinforced aluminum foam.

foam at 60% strain reveals that the base composition (AF02) outperforms all biochar-reinforced variants (AFB01, AFB02, and AFB03). AF02 exhibits a significantly higher energy absorption capacity, reaching approximately 2.8 MJ/m^3 at a stress of around 13 MPa, with a smooth and continuous increase, indicating superior load-bearing capability. In contrast, the biochar-reinforced foams show lower energy absorption and earlier densification, with stress values plateauing around 3–4 MPa. Among them, AFB01 demonstrates the highest absorption but is still far below AF02. This suggests that biochar reinforcement may reduce the foam's toughness or ductility, possibly due to increased porosity or weaker cell walls. Further microstructural analysis is needed to understand these effects, and optimizing biochar content or combining it with additional reinforcements like $CaCO_3$ or Al_2O_3 may enhance performance. Additional mechanical testing at different strain levels could also provide deeper insights into the role of biochar in aluminum foam composites.

Biochar-reinforced aluminum foam electrochemical characterization

The corrosion resistance of biochar-reinforced aluminum foam samples (AFB01, AFB02, and AFB03) was investigated in comparison to the optimized Phase-I aluminum foam sample (AF02), which contains 3% $CaCO_3$ and 1% Al_2O_3, as listed in Table 7. Figure 21 illustrates the Tafel curves, highlighting that sample AF02 has a significantly higher corrosion current density (I_{corr}) of approximately 690.56 µA/cm^2, corresponding to a high corrosion rate of 2086.04 mpy. This behavior indicates that AF02 has limited corrosion resistance without biochar reinforcement. In contrast, biochar-reinforced samples exhibit lower Icorr values, indicating enhanced corrosion resistance. Notably, sample AFB01, with a biochar content of 1%, shows the lowest I_{corr} (77.83 µA/cm^2) and a corrosion rate of only 235.12 mpy, suggesting that even a small addition of biochar can greatly improve corrosion resistance. However, as biochar content increases to 2% and 3% in samples AFB02 and AFB03, the corrosion rate slightly rises to 320.74 mpy and 579.7 mpy, respectively. This suggests that while biochar enhances corrosion protection at low concentrations, higher biochar levels may introduce microstructural changes that

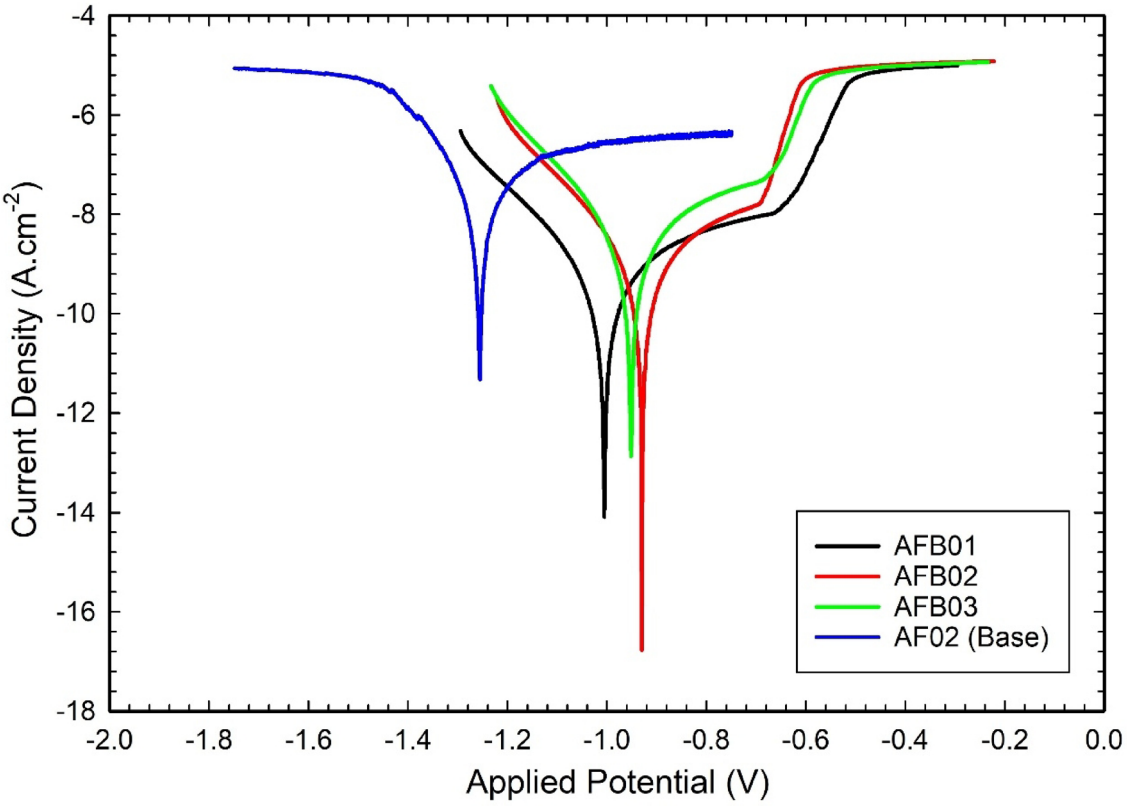

Fig. 21. Anodic and cathodic linear polarization curve of biochar-reinforced aluminum foam.

slightly compromise this protection. Overall, AFB01 demonstrates the optimal balance of biochar content, achieving the best corrosion resistance among the samples tested.

SEM analysis, presented in Fig. 22, further illustrates the corrosion behavior across these samples. The AF02 sample, containing only $CaCO_3$ and Al_2O_3, shows substantial surface degradation following corrosion, including enlarged pores and increased surface roughness, indicating its limited corrosion resistance. Conversely, AFB01, with 1% biochar, displays less surface degradation and more stable structural integrity. With 2% biochar, AFB02 demonstrates an even more stable pore structure and reduced surface defects, indicating improved corrosion resistance. Finally, AFB03, with 3% biochar, exhibits the most minimal surface roughness and the best-preserved pore structure, suggesting that increased biochar content enhances structural integrity and limits corrosion propagation. However, slight increases in corrosion rates were observed electrochemically.

According to published research, pyrolysis temperature and the degree of graphitization determine the conductivity of biochar. Additionally, the biochar is less conductive when made below 600 °C[49,50]. The corrosion characteristics of metallic foam are also significantly influenced by the conductivity of the reinforcing material. Because the biochar in our study was synthesized at 500 °C, the degree of graphitization was minimal. Similarly, the non-conductive and inert character of alumina also contributes to and intensifies this impact. This is the primary reason why adding biochar to aluminum foam improves its corrosion resistance[51].

Figure 23 provides SEM and EDS analyses of the biochar-reinforced aluminum foams, emphasizing the crucial role of carbon in boosting corrosion resistance. Carbon was found to comprise 52.81 wt.% and 66.81 at% of the sample matrix, demonstrating the effective integration of biochar within the aluminum foam. It is noteworthy that the incorporation of biochar across all compositions AFB01, AFB02, and AFB03 results in the formation of a protective barrier. This barrier efficiently shields the aluminum surface by allowing NaCl solution to penetrate, hence increasing corrosion-resistant properties. This phenomenon is known as the carbon barrier effect, which is another reason biochar-reinforced aluminum foam shows better corrosion resistance properties. The barrier impedes the NaCl until it is breached, at that point NaCl attacks the aluminum foam, resulting in pitting corrosion. Carbon contributes to corrosion protection by acting as a physical barrier that fills surface defects, thus inhibiting the penetration of corrosive agents and the initiation of damage. Furthermore, carbon's uniform distribution smooths the surface, reducing imperfections that can act as sites for corrosion. From an electrochemical perspective, carbon acts as a cathode in micro corrosion cells, shifting the corrosion potential to more positive values and thereby reducing the overall corrosion rate. The introduction of biochar also promotes controlled pore size within the foam, which can distribute stress more evenly, adding to the material's structural longevity. The presence of oxygen in the EDS analysis indicates the formation of protective oxides, while intermetallic compounds, including trace elements such as silicon, calcium, and iron, further reinforce the foam's stability. These physical, structural, and electrochemical effects of biochar reinforcement collectively

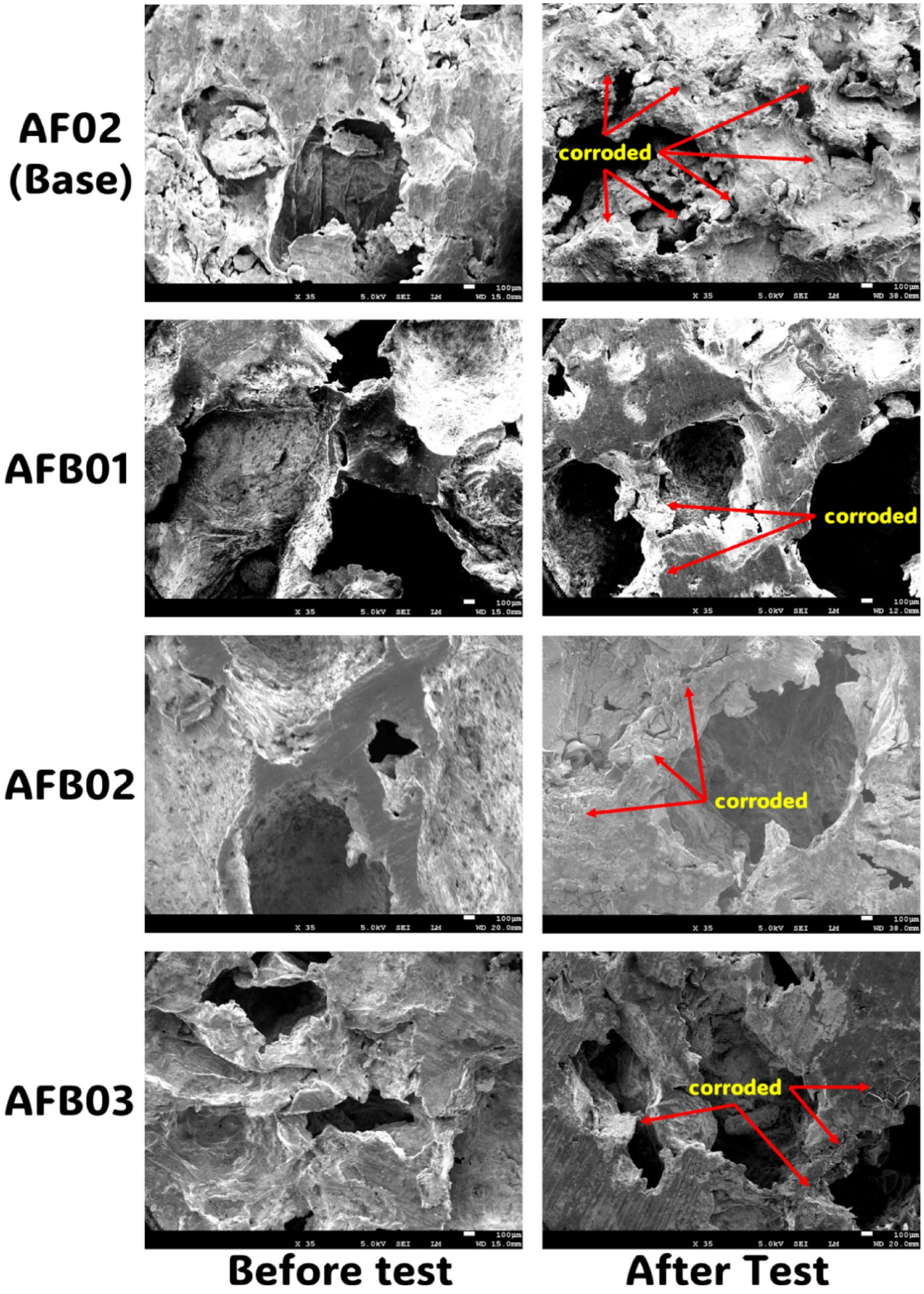

Fig. 22. SEM of fabricated biochar-reinforced aluminum foam before corrosion and after corrosion.

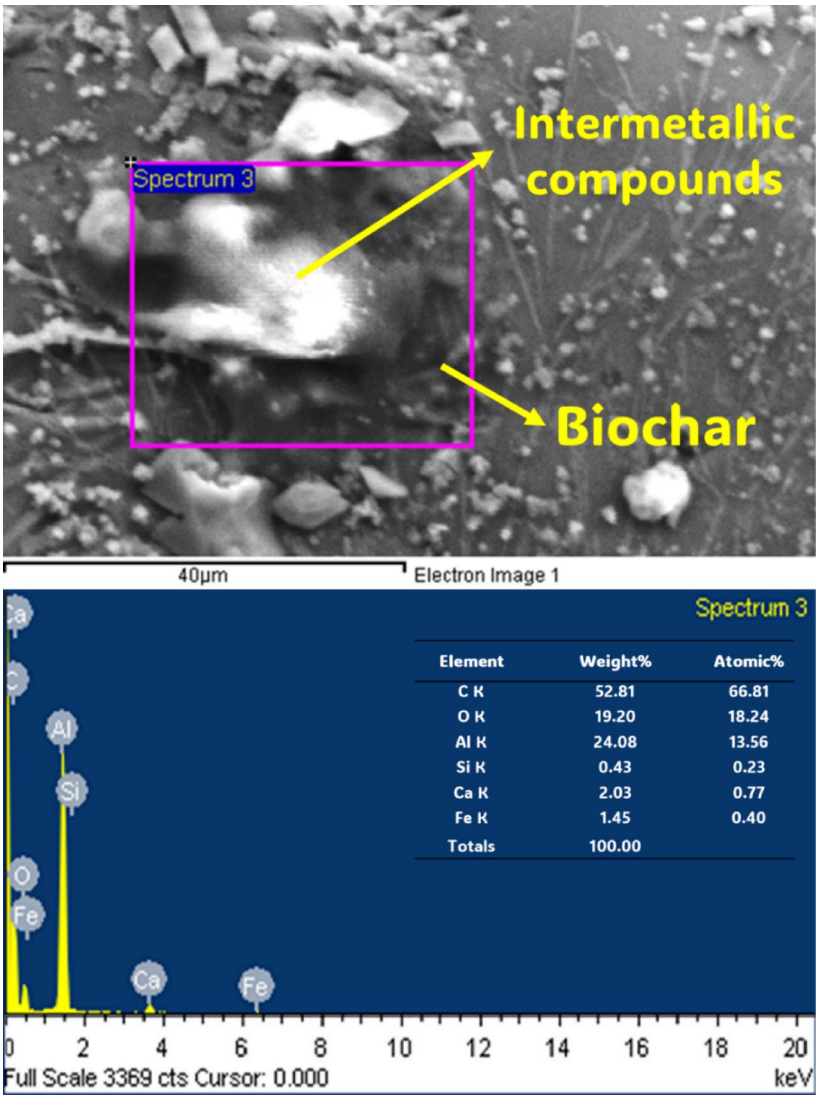

Fig. 23. SEM and EDX analysis of biochar-reinforced aluminum foam.

Compositions	Specific wear rate (mm^3/N m)	Porosity%
AF02 (optimized from phase-I)	0.078 ± 0.003	78.9 ± 1.19
AFB01	0.085 ± 0.006	82.96 ± 1.31
AFB02	0.103 ± 0.005	86.10 ± 1.61
AFB03	0.109 ± 0.007	86.74 ± 1.63

Table 8. Specific wear rate and porosity% of biochar-reinforced aluminum foam.

enhance both the strength and corrosion resistance of aluminum foams, with biochar reinforcement emerging as an effective strategy to extend the material's durability in corrosive environments[6,52].

Biochar-reinforced aluminum foam reciprocating tribology tests

Table 8 presents a clear correlation between porosity percentage and specific wear rate in biochar-reinforced aluminum foams. As the porosity increases from AF02 (78.9%), which is optimized from previous compositions to AFB03 (86.74%), the specific wear rate rises from 0.078 mm^3/N·m to 0.109 mm^3/N·m. This trend indicates that higher porosity enhances wear susceptibility, as graphically represented in Fig. 24. The incorporation of biochar, which has a porous structure and carbon content, significantly affects the overall porosity of the aluminum matrix. While increased porosity can reduce weight, it compromises the material's structural integrity, making it more prone to wear. The larger voids created by biochar exposure increase the surface area available for wear processes, leading to greater material detachment under mechanical stress. Additionally, the carbon content may

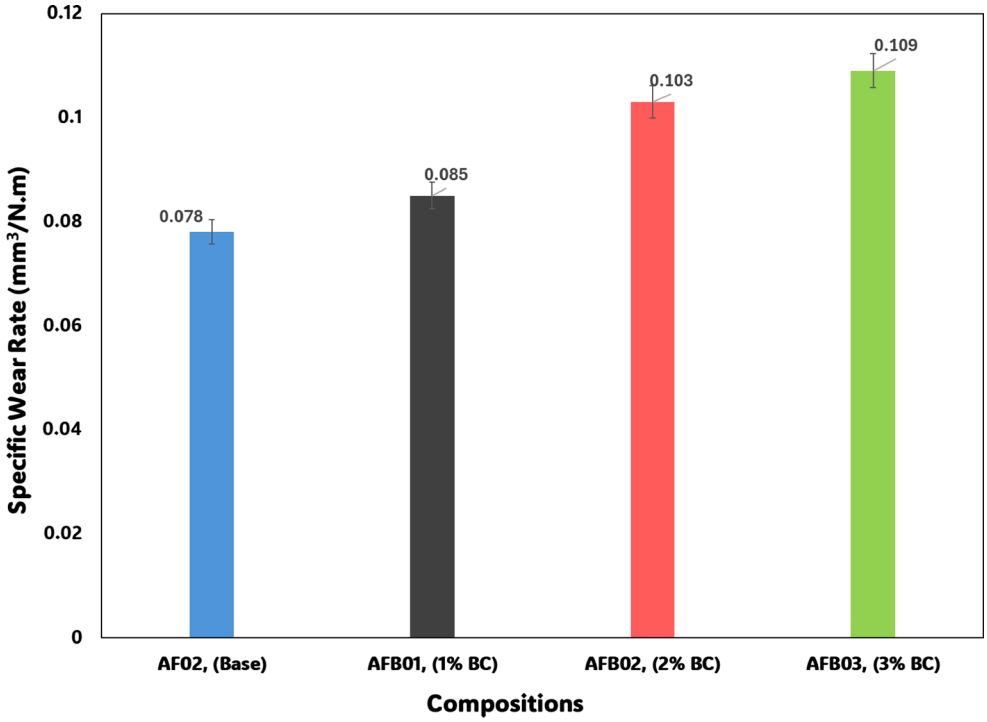

Fig. 24. Histogram of specific wear rate of biochar-reinforced aluminum foam.

Compositions	Microhardness	Porosity%
AF02 (optimized from phase-I)	34 ± 2.91	78.9 ± 1.19
AFB01	36 ± 5.15	82.96 ± 1.31
AFB02	34.8 ± 0.84	86.10 ± 1.61
AFB03	35.8 ± 2.28	86.74 ± 1.63

Table 9. Microhardness and porosity% of biochar-reinforced aluminum foam.

introduce weak points within the aluminum matrix, facilitating crack initiation and propagation, which further elevates the wear rate. Thus, while biochar enhances lightweight characteristics, it also necessitates a careful balance to maintain adequate wear resistance. The findings emphasize the need for optimizing biochar content in aluminum foams to improve performance in applications where wear resistance is essential.

Biochar-reinforced aluminum foam microhardness measurement

Table 9 highlights the relationship between microhardness and porosity in biochar-reinforced aluminum foams, comparing the optimized composition from Phase-I (AF02) with biochar-modified compositions (AFB01, AFB02, and AFB03). AF02, with 3% $CaCO_3$ and 1% Al_2O_3, exhibits a microhardness of 34 HV and a porosity of 78.9%, establishing it as the baseline for performance. According to the literature, as the porosity% rises, the hardness decreases[53]. In addition, the research mentions that adding biochar to the aluminum matrix hardness might boost it by up to 15%[6]. Similar to metal foam, the hardness increases when biochar is applied as reinforcement; however, the hardness immediately declines when the porosity % of biochar-reinforced aluminum foam increases. When biochar is introduced, as seen in AFB01, AFB02, and AFB03, a noticeable increase in porosity is observed, ranging from 82.96% in AFB01 to 86.74% in AFB03. Despite the increase in porosity, which generally reduces material strength, the microhardness values remain relatively stable, with a slight peak of 36 HV in AFB01. This could be attributed to the reinforcing effect of biochar's carbon content, which enhances the material's hardness by improving its load-bearing capability. However, the rise in porosity with increasing biochar content also suggests a compromise in structural integrity. While AFB01 shows a slight improvement in hardness, the increasing porosity in AFB02 and AFB03 indicates that higher biochar content may negatively impact the foam's overall mechanical stability. The challenge lies in balancing the beneficial effects of biochar reinforcement with the potential drawbacks of increased porosity. This data suggests that biochar improves microhardness to an extent but also highlights the importance of optimizing the biochar content to maintain structural integrity. A graphical representation of these trends can be seen in Fig. 25. The material becomes less hard because of an increase in interparticle spacing[54–56].

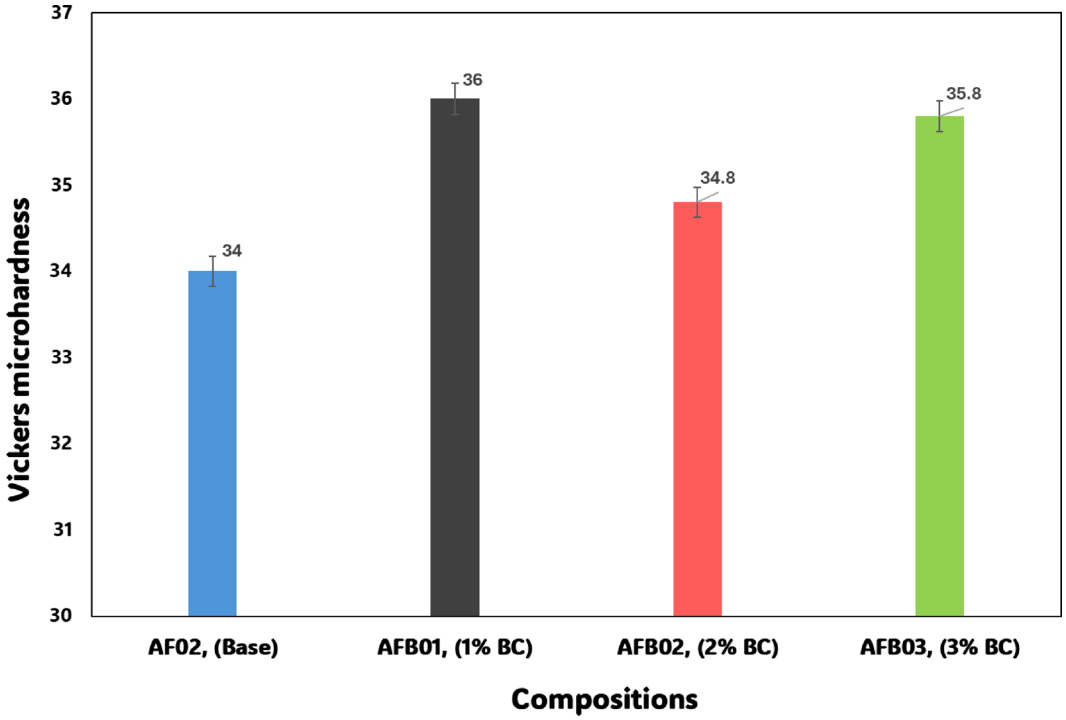

Fig. 25. Histogram of microhardness of biochar-reinforced aluminum foam.

As per our research results, the addition of biochar improved the corrosion resistance of the metallic foam. The carbon-rich structure of biochar acted as a protective barrier, limiting electrolyte penetration and reducing corrosion rate. while nano-reinforcements enhance strength, wear resistance, and stability, resulting in a synergistic improvement in overall mechanical performance. Incorporating 1% to 3% biochar into aluminum foam enhances corrosion resistance and is applicable in lightweight uses in automotive, aerospace, and construction. At a societal level, it ensures the reuse of biomass, decreases dependency on non-renewables, and ensures sustainable development. Conocarpus biochar is a locally available and cost-effective alternative to commercial carbonaceous materials in Saudi Arabia due to its ease of availability and cheap production costs. Conocarpus, which is widely planted in urban construction and landscaping projects around the country, is suitable for sustainable harvesting and conversion into biochar, saving raw material costs. This geographical sourcing advantage increases the economic viability of employing Conocarpus biochar in composite goods, resulting in more sustainable use of waste biomass[57].

Conclusion

This study investigated the reinforcement of closed-cell aluminum foam with Conocarpus-based biochar using the liquid metallurgy process, and its impact on foam morphology, mechanical behavior, wear, microhardness, and corrosion resistance was explored. The corrosion behaviour was evaluated under a 3.5% NaCl solution. Lower concentrations of biochar (1–2 wt.%) exhibit improved corrosion resistance by up to 88.8% via a carbon barrier effect that suppressed electrochemical activity as compared to base composition (AF02). Improvement in microhardness of 5.88% at 1 wt.% biochar was evaluated. This indicates that biochar enhanced durability with no major structural compromise. However, higher biochar (3–4 wt.%) posed processing and performance problems. The inherent porosity of biochar increased overall foam porosity, leading to pore coalescence and the formation of bigger, irregular pores, disrupting cell uniformity. These morphological defects acted as stress concentrators, severely undermining mechanical properties like compressive offset stress, plateau stress, and energy absorption, dropping up to 68.8% at 3 wt.% and even leading to cell collapse at 4 wt.%. In addition, the wear resistance decreased at high biochar percentages. Low biochar concentrations offer an attractive avenue to enhance corrosion resistance and surface hardness of lightweight aluminum foams. Biochar concentrations above 2 wt.% pose a clear trade-off between functional enhancement and mechanical stability. Ideal processing routes for homogeneous biochar dispersion and foam stability are highlighted by these findings. Future work needs to examine hybrid or graded reinforcements to mitigate stress concentration effects and broaden the applicability of the material. Overall, this study establishes a baseline for the application of biochar as a sustainable reinforcement for aluminum foam, offering a balanced perspective on its potential for automotive, aerospace, and structural applications.

Data availability

The data sets used and/or analysed during the current study are available from the corresponding author on reasonable request.

Received: 26 May 2025; Accepted: 4 November 2025
Published online: 21 November 2025

References

1. De Meller, M. A. Produit métallique pour l'obtention d'objets laminés, moulés ou autres, et procédés pour sa fabrication. *French Pat.* **615**(147), 1926 (1925).
2. Wang, N. et al. Compressive performance and deformation mechanism of the dynamic gas injection aluminum foams. *Mater. Charact.* **147**, 11–20 (2019).
3. Wang, X. F., Wang, X. F., Wei, X., Han, F. S. & Wang, X. L. Sound absorption of open celled aluminium foam fabricated by investment casting method. *Mater. Sci. Technol.* **27**(4), 800–804 (2011).
4. Sutygina, A., Betke, U. & Scheffler, M. Open-cell aluminum foams by the sponge replication technique. *Materials* **12**(23), 3840 (2019).
5. Kashihara, M., Hyun, S. K., Yonetani, H., Kobi, T. & Nakajima, H. Fabrication of lotus-type porous carbon steel by unidirectional solidification in nitrogen atmosphere. *Scr. Mater.* **54**(4), 509–512 (2006).
6. Alnaser, I. A. Tailoring the mechanical strength and corrosion resistance of aluminum matrix composites through biochar reinforcement at varied weight percentages. *Sci. Rep.* **14**(1), 19875. https://doi.org/10.1038/s41598-024-70889-3 (2024).
7. Abdo, H. et al. Ecofriendly biochar as a low-cost solid lubricating filler for LDPE sustainable biocomposites: Thermal, mechanical, and tribological characterization. *Int. J. Polym. Sci.* **2023**, 13. https://doi.org/10.1155/2023/2445472 (2023).
8. Lu, Y. et al. Biochar implications for the engineering properties of soils: A review. *Sci. Total Environ.* **888**, 164185. https://doi.org/10.1016/j.scitotenv.2023.164185 (2023).
9. Zhang, A. et al. Valorization of fruit waste by biochar production via thermochemical conversion—A mini-review. *J. Anal. Appl. Pyrolysis* **182**, 106688. https://doi.org/10.1016/j.jaap.2024.106688 (2024).
10. Safarian, S. Performance analysis of sustainable technologies for biochar production: A comprehensive review. *Energy Rep.* **9**, 4574–4593. https://doi.org/10.1016/j.egyr.2023.03.111 (2023).
11. Sobhan, A. et al. Development and characterization of a novel activated biochar-based polymer composite for biosensors. *Int. J. Polym. Anal. Charact.* **26**, 1–17. https://doi.org/10.1080/1023666X.2021.1921497 (2021).
12. Afshar, M. & Mofatteh, S. Biochar for a sustainable future: Environmentally friendly production and diverse applications. *Results Eng.* **23**, 102433. https://doi.org/10.1016/j.rineng.2024.102433 (2024).
13. Madgule, M., Sreenivasa, C. & Borgaonkar, A. Aluminium metal foam production methods, properties and applications—A review. *Mater. Today Proc.* **77**, 673. https://doi.org/10.1016/j.matpr.2022.11.287 (2023).
14. Papantoniou, I. G., Pantelis, D. I. & Manolakos, D. E. Powder metallurgy route aluminium foams: A study of the effect of powder morphology, compaction pressure and foaming temperature on the porous structure. *Procedia Struct. Integrity* **10**, 243–248. https://doi.org/10.1016/j.prostr.2018.09.034 (2018).
15. Hassan, A. & Alnaser, I. A. *A Review of Different Manufacturing Methods of Metallic Foams* (ACS Omega, 2024).
16. Afifi, H., Ahmed, M. & El-Galy, I. Characterization of closed-cell aluminum foams produced by melt-based technique. *Int. Conf. Appl. Mech. Mech. Eng.* **17**, 1–15. https://doi.org/10.21608/amme.2016.35187 (2016).
17. Singh, N., Sethuraman, B., Rathore, R., Namdeo, A. & Kaimkuriya, A. Multi-criteria decision-making technique for optimal material selection of AA7075/SiC composite foam using COPRAS technique. *J. Mines Met. and Fuels* https://doi.org/10.18311/jmmf/2023/34005 (2023).
18. M. F. Ashby *et al.*, "Metal Foams: A Design Guide," (2000). Available: https://api.semanticscholar.org/CorpusID:121139196
19. Miyoshi, T., Itoh, M., Akiyama, S. & Kitahara, A. ALPORAS aluminum foam: Production process, properties, and applications. *Adv. Eng. Mater.* **2**(4), 179–183. https://doi.org/10.1002/(SICI)1527-2648(200004)2:4%3c179::AID-ADEM179%3e3.0.CO;2-G (2000).
20. Rajak, D., Mahajan, N. & Das, S. Fabrication and investigation of influence of $CaCO_3$ as foaming agent on Al-SiCp foam. *Mater. Manuf. Process.* **34**, 379. https://doi.org/10.1080/10426914.2018.1532093 (2018).
21. Hosseini, S. M., Habibolahzadeh, A., Králík, V., Petráňová, V. & Němeček, J. Nano-SiCp effects on the production, microstructural evolution and compressive properties of highly porous Al/$CaCO_3$ foam fabricated via continual annealing and roll-bonding process. *Mater. Sci. Eng. A* **680**, 157–167. https://doi.org/10.1016/j.msea.2016.10.091 (2017).
22. Bisht, A., Gangil, B. & Patel, V. K. Selection of blowing agent for metal foam production: A review. *J. Met. Mater. Miner.* **30**(1). https://doi.org/10.55713/jmmm.v30i1.597 (2020).
23. Matijasevic-Lux, B. *Characterisation and Optimisation of Blowing Agent for Making Improved Metal Foams*. (2006). https://doi.org/10.14279/depositonce-1314.
24. Biban, L. et al. Adhesion and wear behaviour of bagasse biochar reinforced epoxy composite. *Mater. Today Proc.* https://doi.org/10.1016/j.matpr.2023.02.441 (2023).
25. Zhang, G., Zhu, X., Yu, M. & Yang, F. Electrochemical activation of peroxymonosulfate using chlorella biochar modified flat ceramic membrane cathode for berberine removal: Role of superoxide radical and mechanism insight. *Sep. Purif. Technol.* **318**, 124002. https://doi.org/10.1016/j.seppur.2023.124002 (2023).
26. Das, C., Tamrakar, S., Kiziltas, A. & Xie, X. Incorporation of biochar to improve mechanical, thermal and electrical properties of polymer composites. *Polymers* **13**, 2663. https://doi.org/10.3390/polym13162663 (2021).
27. Uram, K., Kurańska, M., Andrzejewski, J. & Prociak, A. Rigid polyurethane foams modified with biochar. *Materials* **14**, 5616. https://doi.org/10.3390/ma14195616 (2021).
28. Jannet, S. et al. Effect of neem seed biochar on the mechanical and wear properties of aluminum metal matrix composites fabricated using stir casting. *Mater. Today Proc.* **56**, 1507–1512. https://doi.org/10.1016/j.matpr.2021.12.572 (2022).
29. Praveen, K., Raja, R., Jannet, S. & George, L. Investigation on the machinability of biochar reinforced AA5083 metal matrix composites fabricated by stir casting technique. *Eng. Res. Express* **6**(1), 015016. https://doi.org/10.1088/2631-8695/ad101f (2024).
30. Andrews, E., Sanders, W. & Gibson, L. J. Compressive and tensile behaviour of aluminum foams. *Mater. Sci. Eng. A* **270**(2), 113–124. https://doi.org/10.1016/S0921-5093(99)00170-7 (1999).
31. Ali, H., Gabora, A., Naeem, M. A., Kalácska, G. & Mankovits, T. Effect of the manufacturing parameters on the pore size and porosity of closed-cell hybrid aluminum foams. *Int. Rev. Appl. Sci. Eng.* **12(3)**, 230–237. https://doi.org/10.1556/1848.2021.00262 (2021).
32. I. ISO, "Mechanical testing of metals—Ductility testing—Compression test for porous and cellular metals, 2011," *Google Scholar*, (2011).
33. Mankovits, T., Varga, T. A., Manó, S. & Kocsis, I. Compressive response determination of closed-cell aluminium foam and linear-elastic finite element simulation of μCT-based directly reconstructed geometrical models. *Strojniški vestnik J. Mech. Eng.* **64**(2), 105–113 (2018).
34. Naeem, M. A., Gábora, A. & Mankovits, T. Influence of the manufacturing parameters on the compressive properties of closed cell aluminum foams. *Period. Polytech. Mech. Eng.* **64**(2), 172–178. https://doi.org/10.3311/PPme.16195 (2020).
35. Sharma, S. et al. Significance of the powder metallurgy approach and its processing parameters on the mechanical behavior of magnesium-based materials. *Nanomaterials* **15**, 92. https://doi.org/10.3390/nano15020092 (2025).

36. Kolev, M., Drenchev, L., Simeonova, T., Krastev, R. & Kavardzhikov, V. Data on mechanical properties of open-cell AlSi10Mg materials and open-cell AlSi10Mg-SiC composites with different pore sizes and strain rates. *Data Brief* **49**, 109461. https://doi.org/10.1016/j.dib.2023.109461 (2023).
37. Rathore, R., Singh, N., Sinha, A., Panthi, S. & Sharma, A. Mechanical properties of lightweight aluminium hybrid composite foams (AHCFs) for structural applications. *Adv. Mater. Process. Technol.* **8**, 1–15. https://doi.org/10.1080/2374068X.2022.2048498 (2022).
38. Mamudu, U., Hussin, M. R., Santos, J. H. & Lim, R. C. Synthesis and characterisation of sulfated-nanocrystalline cellulose in epoxy coatings for corrosion protection of mild steel from sodium chloride solution. *Carbohydr. Polym. Technol. Appl.* **5**, 100306. https://doi.org/10.1016/j.carpta.2023.100306 (2023).
39. Fernandez-Morales, P., Marulanda-Zapata, L. & Vásquez-Rendón, M. Microstructural and corrosion study of aluminum foams obtained by space holder process using low-cost removable preforms. *J. Appl. Res. Technol.* **19**, 202. https://doi.org/10.22201/icat.24486736e.2021.19.3.1687 (2021).
40. Bisht, A., Gangil, B. & Patel, V. K. Physico-compression, sliding wear and energy absorption properties of Zn/Mg infiltrated closed cell aluminum foam. *Mater. Res. Express* **6**(10), 106583. https://doi.org/10.1088/2053-1591/ab3b80 (2019).
41. Soy, U., Demir, A. & Findik, F. Friction and wear behaviors of Al-SiC-BC composites produced by pressure infiltration method. *Ind. Lubr. Tribol.* **63**(5), 387–393. https://doi.org/10.1108/00368791111155002 (2011).
42. Li, H., Ramezani, M. & Chen, Z. W. Dry sliding wear performance and behaviour of powder bed fusion processed Ti–6Al–4V alloy. *Wear* **440**, 203103 (2019).
43. Vijayakumar, R. et al. Optimization of wear process parameters of Al6061-zircon composites using Taguchi method. *Adv. Mater. Sci. Eng.* **2023**, 1–10. https://doi.org/10.1155/2023/9507757 (2023).
44. Bickham, R., Chan, H. & Ravi, V. Corrosion behavior of a novel material—Open-cell aluminum foam. *Mater. Perform.* **59**, 16–17. https://doi.org/10.5006/mp2020_59_11-16 (2020).
45. Singh, R., Arora, R. & Sharma, J. D. Effect of viscosity enhancing agents on quasi-static compression behavior of aluminum foams. *Mater. Today Proc.* **39**, 1661–1666. https://doi.org/10.1016/j.matpr.2020.06.056 (2021).
46. Hu, G. et al. Compressive properties and energy absorption behavior of 316L steel foam prepared by space holder technique. *Materials* **16**, 1419. https://doi.org/10.3390/ma16041419 (2023).
47. Xia, X., Feng, H., Zhang, X. & Zhao, W. The compressive properties of closed-cell aluminum foams with different Mn additions. *Mater. Des.* **51**, 797–802. https://doi.org/10.1016/j.matdes.2013.05.008 (2013).
48. Xia, X. C. et al. Effects of porosity and pore size on the compressive properties of closed-cell Mg alloy foam. *J. Magnes. Alloys* **1**(4), 330–335. https://doi.org/10.1016/j.jma.2013.11.006 (2013).
49. Alves, Z., Ferreira, N., Figueiredo, G., Nunes, C. & Ferreira, P. Electrically conductive and antimicrobial agro-food waste biochar functionalized with zinc oxide particles. *Int. J. Mol. Sci.* **23**, 8022. https://doi.org/10.3390/ijms23148022 (2022).
50. Park, W. et al. Biochar as a low-cost, eco-friendly, and electrically conductive material for terahertz applications. *Sci. Rep.* **11**(1), 18498. https://doi.org/10.1038/s41598-021-98009-5 (2021).
51. Amirjan, M. & Bozorg, M. Properties and corrosion behavior of Al based nanocomposite foams produced by the sintering-dissolution process. *Int. J. Miner. Metall. Mater.* **25**(1), 94–101. https://doi.org/10.1007/s12613-018-1551-5 (2018).
52. Chen, X. et al. Corrosion behavior of carbon nanotubes-Ni composite coating. *Surf. Coat. Technol* **191**, 351–356. https://doi.org/10.1016/j.surfcoat.2004.04.055 (2005).
53. Salins, S. S., Kumar, S., Shetty, S., Sachidananda, H. K. & Khan, M. S. A. Characterization of the aluminium-based metal foam properties for automotive applications. *Arab. J. Sci. Eng.* **50**(12), 9247–9260. https://doi.org/10.1007/s13369-024-09399-3 (2025).
54. Shukla, A. & Dutta Majumdar, J. Studies on microstructure and mechanical properties of aluminium foam prepared by spray forming route. *Procedia Manuf.* **35**, 861–865. https://doi.org/10.1016/j.promfg.2019.06.032 (2019).
55. Salehi, A., Babakhani, A. & Zebarjad, S. Microstructural and mechanical properties of AL-SiO_2 nanocomposite foams produced by ultrasonic technique. *Mater. Sci. Eng. A* https://doi.org/10.1016/j.msea.2015.04.024 (2015).
56. Lüle Şenöz, G. & Daskesen, R. Effect of B4C amount on the microhardness of AA7075/B4C composite metal foam. *Powder Metall. Metal Ceram.* **61**, 60–69. https://doi.org/10.1007/s11106-022-00295-9 (2022).
57. Al-Wabel, M. I. et al. Conocarpus biochar as a soil amendment for reducing heavy metal availability and uptake by maize plants. *Saudi J. Biol. Sci.* **22**(4), 503–511. https://doi.org/10.1016/j.sjbs.2014.12.003 (2015).

Acknowledgements

The authors express their appreciation to ongoing research funding program (ORF-2025-597) King Saud University, Riyadh, Kingdom of Saudi Arabia.

Author contributions

A.H. and I.A.A. conceptualized and designed the research, conducted experiments, analyzed data. A.H. wrote the main manuscript text. I.A.A. provided supervision throughout the study. All authors reviewed and approved the final manuscript.

Declarations

Competing interests

The authors declare no competing interests.

Additional information

Correspondence and requests for materials should be addressed to I.A.A.

Reprints and permissions information is available at www.nature.com/reprints.

Publisher's note Springer Nature remains neutral with regard to jurisdictional claims in published maps and institutional affiliations.